Canadian Mineralogist
Vol. 29, pp. 1019-1041 (1991)

INVERTED METAMORPHISM WITHIN THE TIBETAN SLAB OF BHUTAN: EVIDENCE FOR A TECTONICALLY TRANSPORTED HEAT-SOURCE

SUSAN M. SWAPP[1] AND LINCOLN S. HOLLISTER
Department of Geological and Geophysical Sciences, Princeton University, Princeton, New Jersey 08544, U.S.A.

ABSTRACT

Within the central portion of the Tibetan slab of Bhutan, early mineral assemblages that formed at model conditions of about 480 - 500°C and 7 kbar were overprinted by a high-temperature penetrative fabric. This fabric, which probably formed during convergence of India with Asia, was later overprinted by mineral assemblages that formed at temperatures up to about 640°C, at about 6 kbar. Above the central portion, in the upper part of the Tibetan slab, syn- to postdeformational mineral assemblages equilibrated at 4 kbar and 620°C after cooling from temperatures of about 700°C. Reaction textures and geothermobarometry indicate high-temperature decompression of the upper portion of the Tibetan slab to about 4 kbar from a higher pressure. The upper portion contains leucogranites that intruded into rocks that previously had been heated past the second sillimanite isograd and had been penetratively deformed. The leucogranites therefore were not the source of heat for the high-temperature upper portion of the slab. Our data from Bhutan suggest that the central portion of the slab was heated by the migmatitic upper portion. We propose that this migmatite was uplifted from lower crustal depths and thrust over the central portion. The proposed thrust-shear probably predates motion on the Main Central thrust. The entire hot package, including the central and upper portions of the Tibetan slab, was rapidly exhumed during and after thrusting.

Keywords: Tibetan slab, inverted metamorphism, thermobarometry, leucogranite, Bhutan.

SOMMAIRE

Des assemblages de minéraux précoces de la portion centrale de la plaque tibétaine au Bhutan, qui se seraient formés à environ 480–500°C et 7 kbar, sont affectés par une déformation homogène de haute température. Cette structure, qui relèverait de la convergence de l'Inde avec l'Asie, a elle-même été modifiée par la formation d'assemblages à 640°C et 6 kbar. Au dessus de cette partie centrale, et donc dans la partie supérieure de la plaque tibétaine, les assemblages de minéraux contemporains de la déformation, ou postérieurs à celle-ci, ont équilibré à 4 kbar et 620°C après avoir refroidi d'une température d'environ 700°C. Les textures de réaction et la thermobarométrie indiquent une décompression à haute température jusqu'à environ 4 kbar dans la partie supérieure de la plaque tibétaine. Ce milieu contient des leucogranites qui recoupent des roches antérieurement chauffées au delà du deuxième isograde de la sillimanite et aussi déformées. Les venues leucogranitiques ne seraient donc pas la source de chaleur requise pour expliquer le métamorphisme de haute température. D'après nos données, le centre de la plaque tibétaine a été chauffé par la partie supérieure de la plaque, migmatitique. Nous croyons que ce socle migmatitique a été transporté de la croûte inférieure et s'est trouvé placé au dessus de la partie centrale. La zone de cisaillement serait plus ancienne que le mouvement le long de la faille principale centrale. Les parties centrale et supérieure juxtaposées de la plaque tibétaine ont été rapidement exhumées pendant et après leur mise en place.

(Traduit par la Rédaction)

Mots-clés: plaque tibétaine, métamorphisme inversé, thermobarométrie, leucogranite, Bhutan.

INTRODUCTION

The crystalline rocks of the Tibetan slab of the high Himalaya (Fig. 1) are generally considered to be a portion of the Indian Shield and its cover rocks, which was uplifted by thrusting along the Main Central and Main Boundary thrusts during the terminal phase of the collision of the Indian subcontinent with Asia (Allègre *et al.* 1984, Molnar 1984, 1986, Windley 1983). The exposed gneiss and migmatite of the Tibetan slab in Bhutan include the metamorphosed equivalents of the Paleozoic platform sedimentary sequence and the underlying Precambrian shield (Gansser 1983).

Following Gansser (1964) and Le Fort (1975), much has been written about the distribution of metamorphic mineral assemblages in the Himalaya. Metamorphic grade increases toward higher structural levels (Banerjee *et al.* 1983, Brunel & Kienast 1986, Frank *et al.* 1973, Gansser 1964, 1983,

[1]Present address: Department of Geology & Geophysics, University of Wyoming, Laramie, Wyoming 82071, U.S.A.

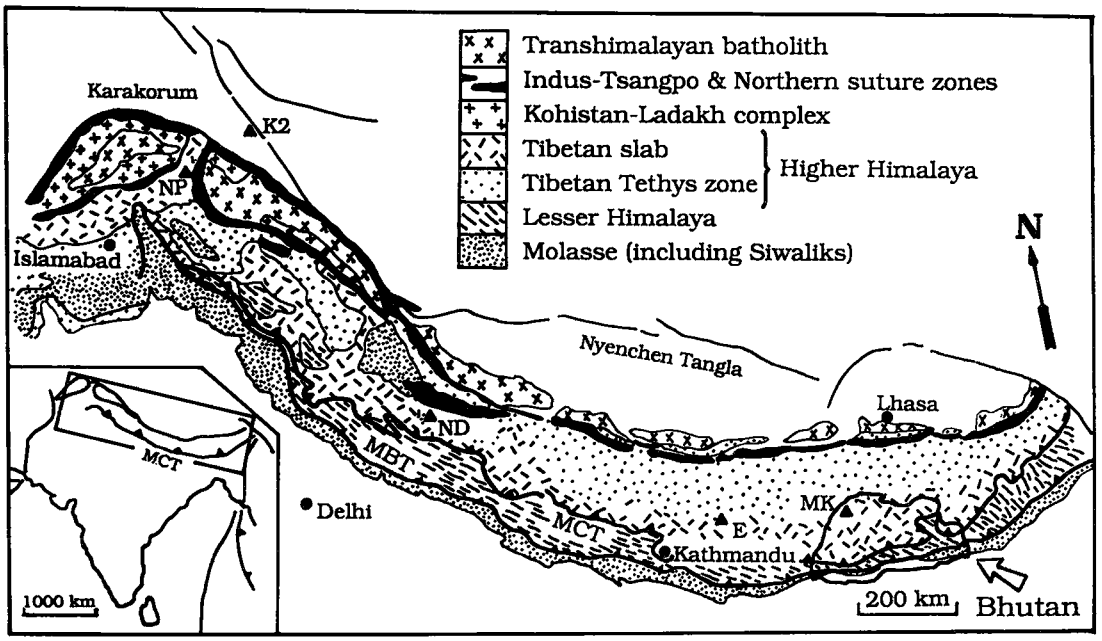

FIG. 1. Generalized geological map of the Himalaya showing the principal geological divisions and the outline of Bhutan. Abbreviations: NP Mount Nanga Parbat, ND Mount Nanda Devi, E Mount Everest, MK Mount Masang Kang, MBT Main Boundary Thrust, and MCT Main Central Thrust. Modified slightly from Barnicoat & Treloar (1989, p. 5).

Hodges *et al.* 1988a, b, Honegger *et al.* 1982, Hubbard 1989, Le Fort 1975, 1986, Mohan *et al.* 1989, Pecher 1989, Searle & Rex 1989, Stäubli 1986, 1989, Treloar *et al.* 1989); such a relationship is commonly referred to as an inverted metamorphic sequence. Brunel & Kienast (1986) and Hodges *et al.* (1988a, b) have questioned that there is a continuous increase of metamorphic grade toward higher structural levels in the central Himalaya based on metamorphic textures and thermobarometry of low-variance assemblages. They conclude that there was an early, high-pressure (M1) metamorphic event that preceded the Main Central thrust, and a later, low-pressure – high-temperature (M2) episode of metamorphism that overprinted M1 mainly in the upper portion of the Tibetan slab. Our new data are consistent with these conclusions.

Pressure–temperature paths determined from compositional zoning of garnet do not give a consistent pattern across or along the Himalaya (Hodges & Silverberg 1988, Le Fort 1986, Hodges *et al.* 1988a, b, 1989, Hubbard 1989, Brunel & Kienast 1986, Pognante & Lombardo 1989, Pecher 1989, Stäubli 1989, Mohan *et al.* 1989, Treloar *et al.* 1989, Chamberlain *et al.* 1989). This is possibly due to the fact that the minerals have been variably affected by retrogression and that high-temperature penetrative deformation is common in the Tibetan slab. Nevertheless, most data suggest that some re-equilibration of minerals occurred at high temperature during or following decompression.

The model of Vidal *et al.* (1982) for the generation of the Himalaya leucogranites calls for overthrusting of a hot Tibetan slab onto lower-grade sediment. According to them, water was generated by dehydration reactions in the footwall of the Main Central thrust during conduction of heat downward from the hot hanging wall (the Tibetan slab). When this water migrated up into the hot Tibetan slab, melting was initiated, and the product of this process was the leucogranites. In addition to the geochemical data reported in Vidal *et al.* (1982) and Honegger *et al.* (1982), the model is supported by the concurrence of intrusion of the leucogranites (at about 20 Ma) with thrusting on the Main Central thrust (Deniel *et al.* 1987, Ferrara *et al.* 1983, Gariépy *et al.* 1985, Schärer *et al.* 1984, 1986, Hubbard & Harrison 1989).

The leucogranites were emplaced after development of the pronounced penetrative fabric that occurs through most of the Tibetan slab (Vidal *et al.* 1982, Honegger *et al.* 1982, Gansser 1964, 1983, Le Fort 1975, 1981, 1986). Their association with

extensive sillimanite + K-feldspar assemblages in the high levels of the Tibetan slab has led some investigators to attribute metamorphism to the intrusion of the leucogranites. However, it is difficult to reconcile the rather sparse occurrence (on average) of the leucogranites with the widespread distribution of sillimanite without additional sources of heat. The alternative, that the leucogranites were the product of high-grade metamorphism, also is difficult to reconcile with the occurrence of both the leucogranites and the sillimanite-grade metamorphism in the higher structural levels of the Tibetan slab and the absence of a similar association in the lower structural levels.

Where stretching lineations are present, they are oriented roughly north–south, parallel to the direction of convergence of India with Asia (Bouchez & Pecher 1981). Most of the kinematic indicators recognized within the Tibetan slab indicate that the direction of transport was top to the south. Ten of twelve of our observations in Bhutan are consistent with this direction of transport.

Abundant felsic igneous sills occur within the Tibetan slab. The age of these bodies is for the most part unknown. A few have been assigned Paleozoic ages (Debon *et al.* 1986, Gariépy *et al.* 1985), which implies a pre-collision igneous history; not enough work has been done on these to rule out syncollisional emplacement for some. The age and origin of these bodies remain largely unknown for the Tibetan slab.

The present study was undertaken within the Tibetan slab in Bhutan (Fig. 1) in order to answer questions pertaining to the relations of fabric

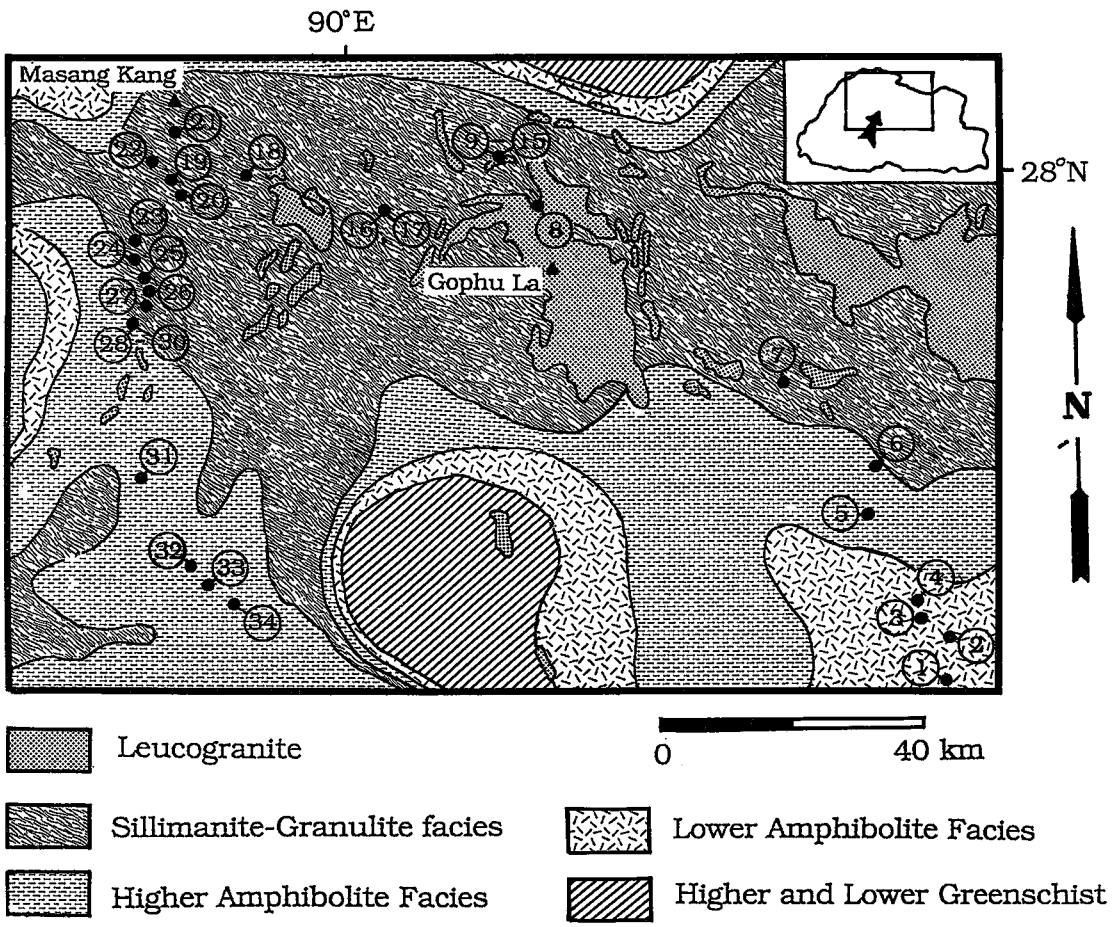

FIG. 2. Study area in Bhutan showing metamorphic facies and major bodies of leucogranite as mapped by Gansser (1983). Also shown are localities for all samples discussed in this report. Sample numbers correspond to sample localities.

development and growth of metamorphic minerals and to constrain the P–T paths of samples from various structural levels. Low-variance assemblages were sought, and we concentrated on defining P–T paths from reactions to reduce the uncertainties involved in using exchange equilibrium in high-grade assemblages (Spear 1991) and in deformed, partially re-equilibrated assemblages. The results of geothermobarometry are presented for comparison.

Bhutan (Figs. 1, 2), a kingdom in the eastern Himalaya, is a country virtually unknown to metamorphic petrologists. Thus, besides adding to the growing body of information on metamorphism of the Himalaya in general, we are able to extend this coverage to the eastern Himalaya. Our samples were collected with reference to the map of Gansser (1983). The only other topical studies done on rocks from Bhutan were those on the leucogranites by Dietrich & Gansser (1981) and by Ferrara *et al.* (1985).

We have established that (1) high-pressure metamorphism preceded the main penetrative deformation, (2) a lower-pressure, high-temperature metamorphism followed this high-pressure metamorphism in the upper portion of the Tibetan slab, and (3) the lower portions of the Tibetan slab were heated to higher temperatures following the penetrative deformation. We propose that thrusting of migmatite over the amphibolite-facies rocks of the lower crustal levels of the Tibetan slab resulted in the additional heating of these rocks. Although this interpretation is a possible solution to the problem of the origin of the enigmatic thermal event in the higher Himalaya (reviewed in Hodges *et al.* 1988a), more work needs to be done to map out the post-deformational prograde (increasing temperature) reaction-textures we have identified in the lower portions of the Tibetan slab in Bhutan.

The metamorphic sequence that we here discuss is wholly within the Tibetan slab (Fig. 2). It does not include the metamorphic discontinuities present along some portions of the Main Central thrust in Bhutan, whose trace was mapped by Gansser (1983) south of the area shown in Figure 2. In Bhutan, nearly the entire length of the Main Central thrust marks a sharp discontinuity in metamorphic grade between the greenschist-facies rocks of the Lesser Himalaya and the amphibolite-facies rocks of the overlying Tibetan slab. Thus, at the erosion level exposed in Bhutan, there is no reported evidence along the Main Central thrust for the thrusting of hot crystalline rock over sedimentary rocks (Gansser 1983).

The possible repetition of metamorphosed platform sedimentary rocks across the Tibetan slab in Bhutan also suggests that there may be significant, unmapped shear-displacements within the Tibetan slab. Although a discrete thrust-zone has not been recognized within the Tibetan slab of Bhutan, the contrast in P–T paths across the Tibetan slab that is identified in this paper strongly implies substantial net displacement across the Tibetan slab. The absence of a recognized discrete shear-zone is possibly the result of the high temperatures within the shear-zone during thrusting, over 600°C, and the fact that strain was presumably distributed across a wide zone.

Regional Geological Setting

The samples described in this report were collected in Bhutan during a 29-day walking traverse that covered about 250 km (Fig. 2). Our samples come from the northern portion of the Tibetan slab. The first leg of the traverse (represented by samples 1–8) was mainly across the strike of the lithologic layering, from elevations near 2500 meters at Bumthang (at location 1 on Fig. 2) to 5300 meters at Gophu La. Samples 9–22 were collected more or less along strike at an elevation of 4000 to 5000 meters within the highest (both structurally and topographically) portion of the Tibetan slab. Samples 23–34 were collected across strike on the return leg, some 100 km west of the first leg.

Gansser (1983) described the rocks in the traverse area as consisting of gneiss, leucogranite, pelitic metasediment, calc-silicate, marble, and pegmatite. All these rock types were seen in the field, but we concentrated on collecting samples of lithologies containing metamorphic porphyroclasts of cordierite, sillimanite, garnet, kyanite, and staurolite. The necessity of reaching a predetermined destination each night left only enough time to collect one or two samples per day, and to make structural measurements.

Foliations along most of the traverse dip gently north or south, but mostly north. The traverse crossed approximately half of the Tibetan slab in Bhutan, or about 8–10 km of structural relief, based on Gansser's estimate of the Tibetan slab in Bhutan being 15 km thick. Unfortunately, reliable topographic maps of the region were unavailable to us. The lack of good maps, and the time constraints of the traverse, precluded precise measurement of the exposed structural relief for the area sampled.

The few lineations measured vary in orientation, but define a weak maximum toward the north-northeast. Lineations defined by sillimanite in the highest structural levels trend east-northeast. Eight of nine megascopic kinematic indicators showed a top-to-the-south direction of tectonic transport.

TABLE 1. MINERALS OBSERVED IN SAMPLES BEARING ALUMINOSILICATE OR CORDIERITE (OR BOTH)

	St	Ky	Ms	Sil	Grt	Bt	Crd	Kfs	Pl	Qtz	Acc
B1		X	X		X	X			X	X	I
B2		X	X		X	X			X	X	I
B4	X	X	X	X	X	X			X	X	PJ
B5	X		X	X	X	X			X	X	
B6	X		X	X	X	X			X	X	I
B7	(g)		X	X	X	X			X	X	
B34			X	X		X		X	X	X	
B32			X	X		X		X	X	X	
B33			†	X	†	X		X	X	X	I
B30			†	(c)	X	X	X	X	X	X	
B27				X	†	X		X	X	X	
B28		(s)	X	X		X	X	X	X	X	H,P
B26				X	X	X	X			X	I
B25			†	X	X	X	X	X	X	X	
B23			†	X				X	X	X	I
B19			†	X	X	X		X	X	X	
B20				X	X	X		X	X	X	
B16			X	X		X		X		X	
B17			X	X		X		X	X	X	
B11			X	X	X	X		X	X	X	M
B12			X	X		X		X	X	X	
B13				X		X			X	X	
B18					X	X	X	X	X	X	I
B22				X	X	X		X	X	X	I,G

Notes: Minerals present only in trace amounts are indicated by "t". Minerals that occur only as inclusions in another mineral are indicated by "(x)", where x is the first letter of the host mineral. Abbreviations (after Kretz 1983): staurolite (St), kyanite (Ky), muscovite (Ms), sillimanite (Sil), garnet (Grt), biotite (Bt), cordierite (Crd), K-feldspar (Kfs), plagioclase (Pl), quartz (Qtz), and accessory phases (Acc), including ilmenite (I), magnetite (M), pyrite (P), hercynite (H), and gahnite (G). In addition to minerals tabulated above, nearly all samples contain allanite or apatite or both. See Figure 2 for sample localities.

These data are consistent with an interpretation that the pervasive penetrative fabric of the Tibetan slab was formed during compression.

We describe and interpret a suite of pelitic rocks (Table 1, Fig. 2) containing assemblages useful for the determination of pressures and temperatures, with textures that constrain the relative timing of deformation and metamorphic reactions. In most cases, the samples contain kyanite or sillimanite. We (1) describe assemblages and textures, (2) summarize mineral chemistry, (3) infer reactions from textural relations and mineral chemistry, and constrain P–T conditions of reaction, (4) determine the timing of reactions relative to deformation, and (5) use mineral chemistry with thermobarometers to constrain relative spatial and temporal variations in pressure and temperature.

It was impossible in the field to collect enough samples to determine whether metamorphic isograds are parallel to the lithologic layering or cut sharply across it. Because Gansser (1983) found that metamorphic grade correlates with structural level, and because in the Himalaya to the west of Bhutan this relationship also is typical, we presume in our discussions that isogradic surfaces are more or less concordant with the lithologic layering. More work in Bhutan should be done to test this inference.

Petrography

Our sample localities are within areas of three metamorphic facies mapped by Gansser (1983; Fig. 2), and we observe assemblages (Table 1) generally consistent with his classification. Gansser (1983) described the following characteristic aluminosilicate-bearing assemblages in his facies:

Facies	Al_2SiO_5-Bearing Assemblage
"Lower Amphibolite"	Kyanite + Garnet + Biotite + Muscovite + Plagioclase + Quartz + Staurolite
"Higher Amphibolite"	Sillimanite + Muscovite + Garnet + Plagioclase + Quartz ± Kyanite ± Staurolite ± K-Feldspar
"Sillimanite Granulite"	Sillimanite + Biotite + Garnet + Plagioclase + K-Feldspar + Quartz + Cordierite + Muscovite + Hercynite

Gansser's "Lower Amphibolite" facies can be characterized by the presence of kyanite or staurolite (or both) and the absence of sillimanite. Sillimanite coexisting with abundant muscovite and quartz (and in some samples with minor K-feldspar) are characteristic of his "Higher Amphibolite" facies, and sillimanite and K-feldspar with little or no muscovite characterize his "Sillimanite Granulite" facies.

All four characteristic aluminosilicate-bearing assemblages occur in our sample suite (Table 1), and their locations are generally consistent with Gansser's metamorphic isograds. Notable exceptions are the occurrences of sillimanite + K-feldspar samples in our suite from the southwestern portion of Figure 2, which is within Gansser's "Higher Amphibolite" facies. With these exceptions, our observations suggest that Gansser's metamorphic facies can be used to help organize the observations presented in this paper.

In addition to the characteristic aluminosilicate-bearing assemblages mapped by Gansser, we found samples containing moderate amounts of muscovite and quartz coexisting with abundant K-feldspar within Gansser's "Higher Amphibolite" and "Sillimanite Granulite" facies (Table 1). The muscovite in these samples is coarse grained and cross-cuts the foliation. This assemblage is not characteristic of any mapped facies and is apparently randomly distributed above the Lower Amphibolite facies; it is concluded in the discussions below that this muscovite formed during cooling.

In this report, we categorize samples according to their approximate structural level within the Tibetan slab: the lower structural levels (LSL), and the higher structural levels (HSL). The assemblages listed in Table 1 and those taken from Gansser's

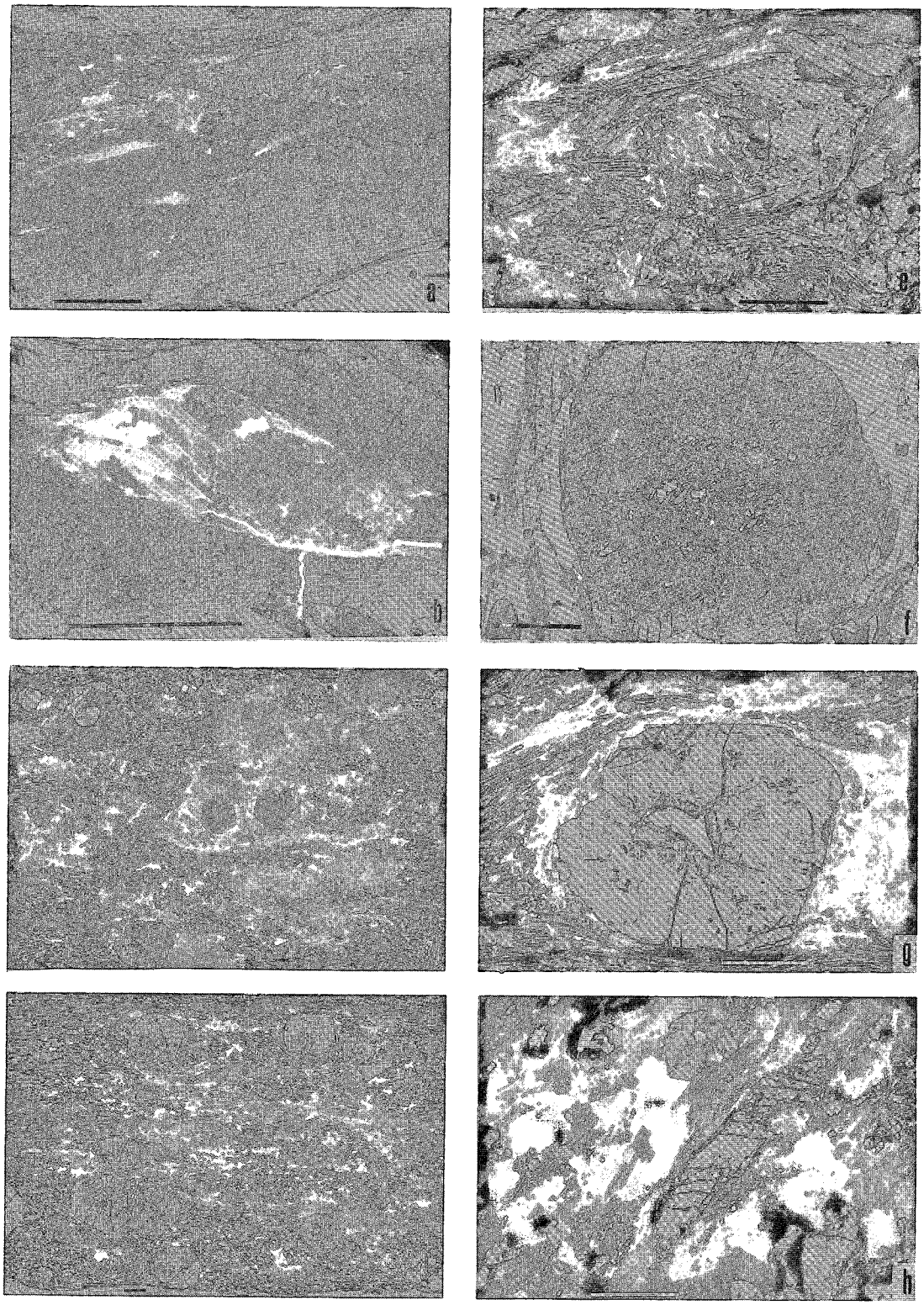

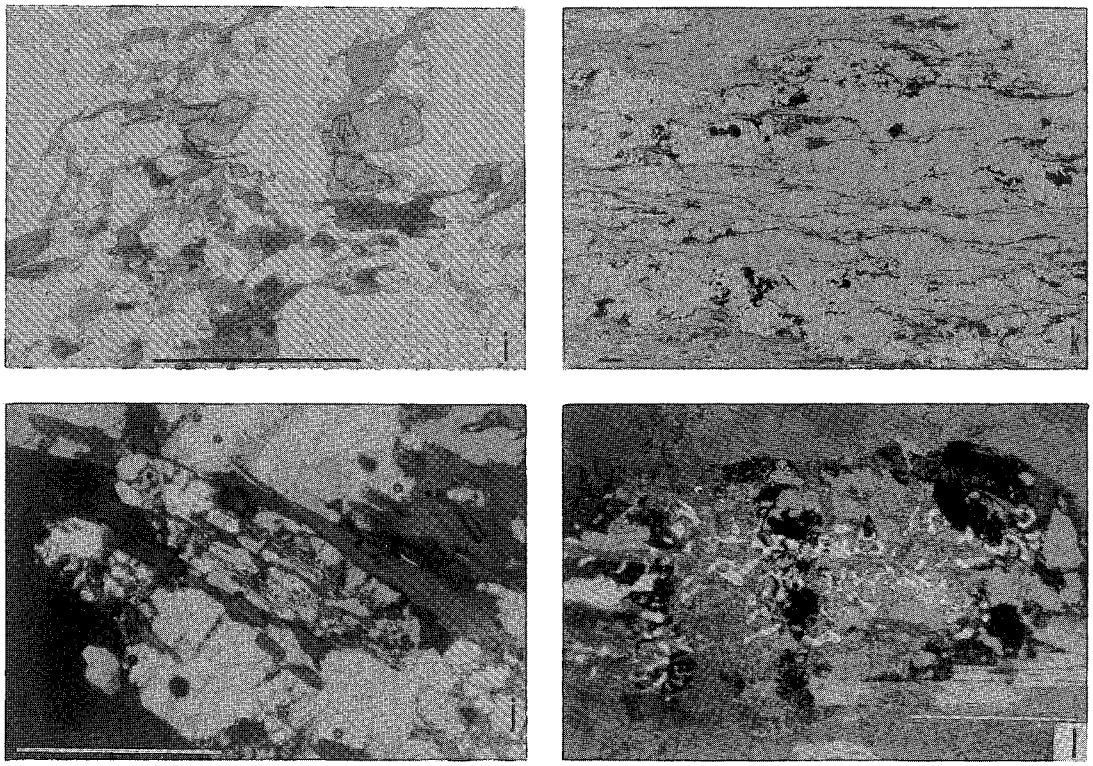

FIG. 3. The photomicrographs were taken in plane-polarized light unless otherwise noted (H, L). The scale bar is 1 mm. Thin sections of all samples were cut parallel to lineation and perpendicular to foliation. A. The small, irregularly shaped high-relief grains forming a subhorizontal trail are fresh staurolite fragments. Muscovite and biotite augen also are present (sample B4). B. Kyanite augen. Abundant biotite occurs in the pressure shadow (sample B2). C. Rounded aggegrates of coarse-grained, unfoliated muscovite + biotite + plagioclase + ilmenite in pseudomorphs after staurolite; most still contain staurolite fragments. The euhedral grains of garnet are mantled by a biotite + fibrolite intergrowth. Both the staurolite pseudomorphs and the biotite–fibrolite mantles are undeformed (see also E); (sample B6). D. Elongate aggregates of coarse-grained muscovite + biotite + plagioclase + ilmenite resemble the pseudomorphs in C in size and mineralogy. Biotite + fibrolite intergrowths are concentrated along foliation planes, in contrast to sample B6, in which they mantle the garnet. Staurolite is present only as inclusions in the garnet (sample B7). E. The high-relief grains near the center of the photo are optically continuous staurolite fragments and are probably remnants of a single larger crystal that has been replaced by an intergrowth of muscovite + biotite + plagioclase + ilmenite. The entire pseudomorph is undeformed (see also C); (sample B6). F. Subhedral garnet with inclusion trails defining what looks like an S and C fabric. The garnet has a narrow, inclusion-free rim, typical of garnet from lower structural levels (sample B1). G. Subhedral garnet with radially oriented inclusions of fibrolite in the outer margin. The garnet is partly surrounded by a biotite–fibrolite mantle. Fibrolite growth apparently postdated deformation (sample B6). H. The large elongate white grain near the center of the photograph is primarily sillimanite. The rounded extinct patch on the right side one-third of the way down from the top is a fragment of kyanite. The habit of the sillimanite–kyanite aggregate suggests that sillimanite formed as a pseudomorph after kyanite (sample B28, crossed polars). I. Small, anhedral grains of garnet with few inclusions are typical of samples from the higher structural levels (sample B22). J. Inclusions of sillimanite needles in cordierite that are separated from the biotite host by the cordierite. K-feldspar also is present. The biotite–cordierite–sillimanite intergrowths are undeformed (sample B30). K. Lensoid cordierite–sillimanite aggregates. The sillimanite needles are oriented parallel to the foliation. Biotite is restricted to the coarse-grained quartzofeldspathic zones, in which sillimanite is absent. K-feldspar also is present. The rock was deformed during or after the breakdown of biotite + sillimanite (sample B26). L. Electron back-scattered image of an undeformed cordierite + hercynite + sillimanite symplectite. The brightest grains are hercynite; these are set in a grey region of cordierite that is distinguished from the surrounding grey regions by the presence of alteration material. The black areas, which are restricted to the symplectite, are holes in the slide. Sillimanite is within the symplectite but is not easily distinguished in the photo; sillimanite is dark grey and occurs near the black holes in the upper right portion of the symplectite, and along the left edge of the photo. The bright grains parallel to and above the scale bar are biotite (sample B28, scale bar 400 μm).

map show that the highest-temperature metamorphic rocks occur to the north of, and structurally above, the lower-grade rocks.

Lower Structural Levels (LSL)

The most common aluminosilicate-bearing assemblage from the LSL is kyanite + garnet + biotite + muscovite + plagioclase + quartz + staurolite + fibrolitic sillimanite. Kyanite is restricted to rocks from the southeastern region of the study area, and fibrolite is rare in these rocks. All these samples are strongly foliated, and both kyanite and staurolite form augen structures or are intensely comminuted along foliation planes (Figs. 3a, b). Crystallization of kyanite and staurolite must have been pre- or synkinematic, but definitely not postkinematic.

Staurolite is unaltered and apparently a stable phase only in the samples where it occurs with kyanite. In other samples, staurolite augen are partially to completely replaced by intergrowths of muscovite + biotite + plagioclase + ilmenite; smaller fragments in the same rocks are surrounded by a less distinct mantle consisting primarily of muscovite (Figs. 3c, d, and e). The larger, partial pseudomorphs after staurolite approach 7 mm in diameter. The pseudomorphs are undeformed in samples B4, 5, and 6 (Figs. 3c, e). A sample from a slightly higher structural level (B7) contains staurolite only as inclusions in garnet, but elongate concentrations of muscovite + biotite + plagioclase + ilmenite, of overall volume and grain size comparable to the pseudomorphs after staurolite at slightly lower levels, occur in this sample (Fig. 3d). These structures are interpreted to be slightly to moderately deformed staurolite pseudomorphs.

The pseudomorphs after staurolite are sensitive indicators of penetrative deformation and are useful in constraining the relative timing of deformation and of the staurolite-consuming reaction across a small portion of the LSL. The staurolite-consuming reaction must be largely or entirely postkinematic in staurolite-bearing samples from the lower structural levels, where the pseudomorphs are undeformed, and synkinematic in slightly higher structural levels, where the pseudomorphs are slightly to moderately deformed. We argue below that the staurolite pseudomorphs formed in response to an increase of temperature during and following penetrative deformation.

Garnet in the LSL occurs as relatively large euhedral to subhedral crystals, with an inclusion-clouded core and clear overgrowth. The inclusions in the garnet core are mostly quartz; also common as inclusions are plagioclase, biotite, ilmenite, muscovite, tourmaline, and staurolite. The distribution of inclusions in the central portion of garnet grains in samples from the LSL define what appear to be S and C fabrics (Fig. 3f). (This thin section, as all others illustrated in Figure 3, is cut parallel to lineation and perpendicular to foliation.) The margin of garnet grains from the structurally highest portions of the LSL is free of inclusions, except for volumetrically minor ilmenite and radially oriented fibrolite inclusions (Fig. 3g). These textures indicate a period of growth of sillimanite and garnet in the absence of penetrative deformation, and suggest that the sillimanite grew after the period of penetrative deformation indicated by the fabric preserved in the core of the grains.

In the samples that contain undeformed pseudomorphs of staurolite, garnet crystals are surrounded by a halo consisting of intergrowths of unfoliated biotite + fibrolite (Figs. 3c, g). Biotite + fibrolite intergrowths also are present in the sample containing deformed pseudomorphs of staurolite; in general, they do not form a mantle around garnet in these samples (Fig. 3d). Biotite, in addition to that occurring with fibrolite in the intergrowths, is, in most samples from the LSL, relatively coarse grained, oriented within the planes of foliation, and without inclusions of fibrolite.

Finally, the aluminosilicate-bearing samples from the lower structural levels contain two texturally distinct varieties of muscovite. One variety defines a foliation and is commonly deformed. The second consists of relatively coarse, undeformed muscovite crystals that cross-cut the foliation and apparently postdate penetrative deformation. The latter variety of muscovite is not restricted to staurolite-bearing samples.

Higher Structural Levels (HSL)

The lowest-variance aluminosilicate-bearing assemblages in the HSL include (1) sillimanite + biotite + garnet + plagioclase + K-feldspar + muscovite + quartz; (2) sillimanite + biotite + garnet + plagioclase + K-feldspar + quartz + cordierite, and (3) sillimanite + biotite + plagioclase + K-feldspar + cordierite + hercynite + quartz. The most common assemblage is sillimanite + biotite + garnet + plagioclase + K-feldspar + quartz ± muscovite.

Grains of garnet are generally small (< 1 mm), anhedral, and contain few inclusions. They are commonly mantled by biotite or cordierite or both (Fig. 3i). The small crystals of garnet occur in strings along foliation planes in many samples, suggesting that they were broken apart during deformation. The biotite and cordierite mantles are

undeformed and clearly postdate penetrative deformation.

Cordierite also occurs in lenses containing abundant, coarse sillimanite. In these samples, cordierite is at least in part pre- or syndeformational in origin. The long axes of the lenses and the orientations of the included sillimanite needles are concordant with the foliation (Fig. 3k), and sillimanite and biotite are everywhere separated by cordierite (Figs. 3j, k). In one sample, sillimanite is confined to the cordierite lenses.

A symplectitic intergrowth of cordierite, hercynite and sillimanite is present in one sample (Fig. 3l). This delicate intergrowth clearly postdates deformation.

In addition to inclusions in cordierite, sillimanite is present as aligned coarse needles within the planes of foliation and also randomly oriented within fibrolite mats.

Several samples from the extreme northwest of the HSL have typical peak metamorphic assemblages, but they have textural evidence for lower-temperature deformation, including mosaic quartz with undulose extinction, broken grains of garnet, and bent twins and cleavages in feldspar.

Our petrographic observations indicate that throughout the HSL there is strong textural evidence for several metamorphic reactions that were synchronous with deformation, and for several that postdated deformation.

Reactions Based on Textural Criteria

Staurolite-out reaction, LSL

Following deformation in the LSL, biotite + sillimanite + garnet were produced by a reaction that consumed staurolite. This conclusion is based on (1) the presence of undeformed muscovite + biotite + plagioclase + ilmenite pseudomorphs after staurolite, (2) the occurrence of a garnet rim containing radially oriented fibrolite crystals, and (3) the presence of an undeformed biotite + fibrolite mantle on garnet. In one sample, lensoid aggregates of muscovite + biotite + plagioclase + ilmenite suggest that the staurolite-consuming reaction predated or was coeval with some deformation.

Guidotti (1974) and Foster (1977, 1981, 1983) described similar textures in rocks from Rangeley, Maine. On the basis of mineral chemistry and textural relations, Guidotti (1974) inferred the following continuous, prograde (increasing temperature) reaction:

[1] Biotite + Muscovite + Staurolite + Quartz = Sillimanite + Biotite (higher Fe/Mg) + Staurolite (higher Fe/Mg) + Garnet + Plagioclase (higher Na/Ca) + H_2O.

Because the textural relations in the Rangeley, Maine rocks are similar to those of the staurolite-bearing samples from the LSL in Bhutan, we assume that the generalized reaction in the Maine rocks is appropriate for the Bhutan rocks.

Guidotti (1974) estimated that because of the limited range of staurolite compositions, this continuous prograde reaction occurred over a narrow range of temperature at conditions near 4 kbar and 600°C, with water pressure near total pressure. Dutrow & Holdaway (1989) experimentally determined the upper thermal stability of staurolite (Fe end-member) + quartz to be approximately 650°C at 3.25 kbar and 680°C at 5 kbar. Based on these studies, and allowing for the lower temperature for the staurolite-breakdown reaction in the presence of muscovite, reaction [1] is plotted on Figure 4 at a position 50°C below the curve of Dutrow & Holdaway (1989).

The steep slope of the curve for reaction [1] in P–T space requires that there was heating of the lowest structural levels. The prograde pseudomorphs after staurolite postdate an episode of deformation (Figs. 3c, e); heating, thus, occurred after deformation. The presence of deformed pseudomorphs in one sample (Fig. 3d) indicates that some deformation outlasted the rise in temperature.

The reaction texture implies a metamorphic field-gradient for the LSL as shown on Figure 4a. This gradient clearly implies heating from north to south, along the transect from location 1 to 7 (Fig. 2), which is inferred also to mean heating from higher structural levels into lower structural levels.

Kyanite-out reaction, HSL

Coarse, lath-shaped aggregates of sillimanite needles that enclose kyanite fragments in one sample (Fig. 3h) indicate the reaction:

[2] Kyanite = Sillimanite

The relict kyanite shows that the HSL had been in the stability field of kyanite.

Cordierite-in reactions, HSL

The three texturally distinct occurrences of cordierite suggest three different cordierite-producing reactions. Two of these reactions apparently postdate deformation of the HSL, whereas the third occurred before or during deformation.

Cordierite replacing garnet in undeformed pseu-

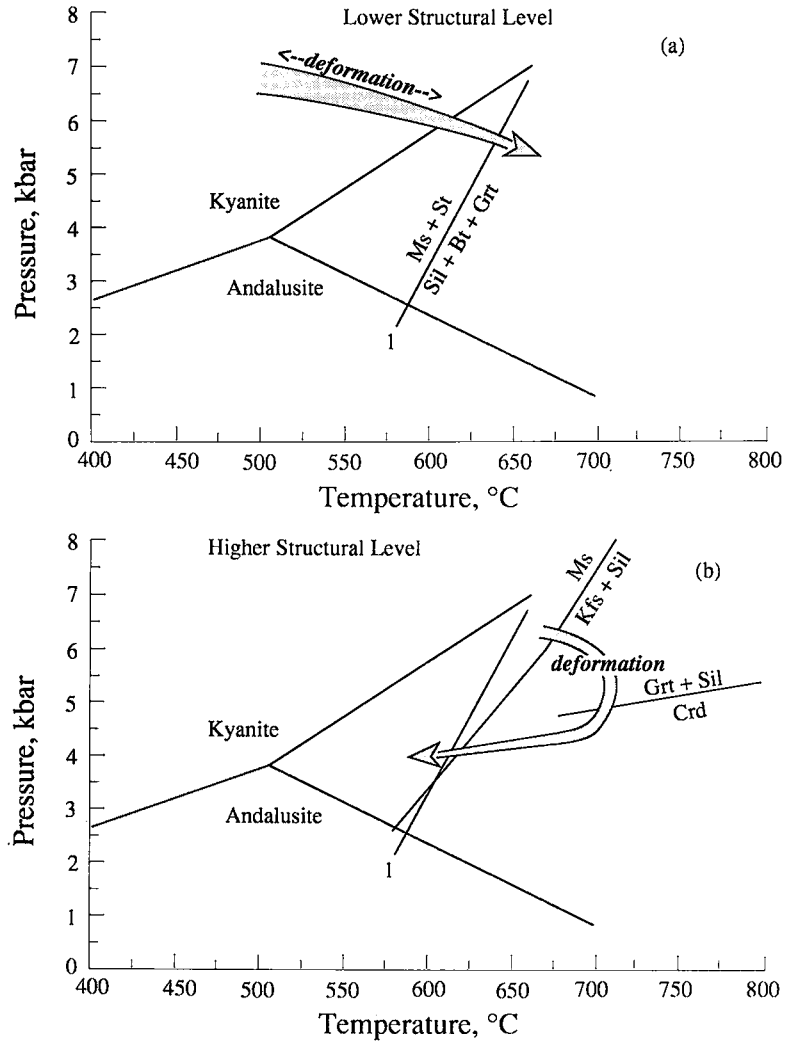

FIG. 4. a. Pressure–temperature path recorded in the lower structural level. Geothermobarometry indicates a starting point at about 7.3 kbar and 500°C. Penetrative deformation was followed by the kyanite-to-sillimanite transition and the reaction of staurolite to garnet + sillimanite (reaction 1). Deformation locally affected the products of reaction 1. Al_2SiO_5 phase diagram from Holdaway (1971); reaction 1 is discussed in the text. The fact that the P–T path crosses reaction 1 at a higher temperature (640°C) than that calculated using the geothermometers (590 – 630°C) is probably an indication of continued cation-exchange during cooling (Spear 1991). b. Pressure–temperature path for the higher structural levels, as inferred from preserved reaction-textures and thermobarometric calculations. Reaction 1 of Fig. 4a is shown for reference. The breakdown of muscovite + quartz (reaction 6) is from Kerrick (1972), at $P(H_2O) = 0.7\ P_{total}$. Reactions 3 and 4 are discussed in the text.

domorphs requires the following garnet-consuming, cordierite-producing reaction:

[3] Garnet + Sillimanite + Quartz + H_2O = Cordierite.

We determined a position of reaction [3] in P–T space (Fig. 4b) according to the method of Berman (1988), with his modifications to the data-base to March, 1990. This calculation includes consideration of H_2O in cordierite, uses the compositions of

minerals given in the next section, and assumes an intermediate value for the partial pressure of H_2O.

In one sample (B26), cordierite forms concordant lenses between well-foliated sillimanite and biotite. This suggests the reaction:

[4] Biotite + Sillimanite + Quartz = Cordierite + K-feldspar + H_2O.

According to Holdaway & Lee (1977), reaction [4] has a positive P–T slope, with the products (as written above) on the high-temperature side.

Finally, the cordierite–hercynite–sillimanite symplectites surrounded by weakly perthitic orthoclase resemble those described by Kenah & Hollister (1983) and Hollister (1982) from the Central Gneiss Complex of the Coast Mountains, British Columbia. There, a symplectite consists of garnet partially replaced by cordierite, ilmenite inclusions within biotite, and sillimanite partially replaced by cordierite and hercynite; this symplectite was interpreted as the product of the arrested reaction:

[5] Biotite + Sillimanite + Garnet = Cordierite + Hercynite + Ilmenite + K-feldspar + H_2O.

The hercynite–cordierite–sillimanite symplectite from the Bhutan suite is apparently a pseudomorph after a completely consumed garnet. Hollister (1982) determined that reaction [5] has a very small positive slope in P–T space. No attempt to calculate an appropriate position for the reaction in our sample is presented, however, because (1) there is no garnet, and (2) the hercynite contains as much as 6% ZnO by weight, and no suitable model is available for calculation of the activity of hercynite. Unless the slope of the reaction curve is profoundly affected by reduced activity of hercynite, the production of cordierite and hercynite from garnet and sillimanite requires either increasing temperature or decompression or both. The preservation of the delicate symplectitic intergrowth implies that the reaction postdated deformation. The presence of K-feldspar and hercynite imply a temperature for the reaction in excess of 700°C (Hollister 1982).

The undeformed halos of cordierite on garnet and the hercynite – cordierite – sillimanite symplectite require that the decompression reactions [3] and [5] postdated deformation in the HSL. Deformed lenses of cordierite separating sillimanite from biotite suggest that reaction [4] was followed by some deformation.

Second sillimanite reaction

Between the LSL and HSL, the disappearance of the coarse-grained muscovite that is oriented parallel to the foliation correlates with a pronounced increase in K-feldspar and coarse, aligned sillimanite. The typical muscovite in the HSL cross-cuts the foliation and clearly postdates deformation. (Similar coarse-grained, unfoliated muscovite also occurs in the LSL.) These textures suggest that the prograde, high-temperature, second sillimanite reaction (Fig. 4b):

[6] Muscovite + Quartz = Sillimanite + K-feldspar + H_2O

predates deformation in the HSL, but that the retrogression that resulted in formation of the late muscovite followed deformation. The presence of the apparent reaction-assemblage across a thermal gradient could also result from variation in composition of muscovite or fluid (Tracy 1978), but the textural distinctions between the two generations of mica argue strongly that they are not coeval.

The retrograde muscovite in the HSL implies the availability of water and rehydration of the rocks. The water was reintroduced late in the metamorphic history, and after penetrative deformation. The weakly zoned garnet of the higher structural levels, and spessartine enrichment of the rim, are typical of garnet heated to at least 650°C, homogenized prior to cooling, and partially re-equilibrated during cooling (Grant & Weiblen 1971, Tracy *et al.* 1976, Woodsworth 1977, Yardley 1977, Tracy 1982).

A P–T path for the HSL that is consistent with our observations is shown on Figure 4b. It contrasts with that of Figure 4a for the LSL in that it reaches higher temperatures, which were maintained during decompression. The higher metamorphic temperatures in the HSL coupled with the evidence for prograde heating to lower temperatures in the LSL, lead to the interpretation that the HSL may have been the heat source for the prograde metamorphism of the LSL. The decompression at high temperature of the HSL implies rapid exhumation while the HSL was heating the LSL.

Mineral Chemistry

Analytical methods

The analyses were carried out on the JEOL 8600 Superprobe at Rutgers University. Counts for each element were collected until 40,000 counts were obtained, or 40 seconds had passed, whichever occurred first. Accelerating voltage was 15 kV for all analyses. The ZAF correction scheme supplied with the JEOL system was used to calculate elemental weight percents, and oxide weight percents were calculated assuming electrostatic

TABLE 2. REPRESENTATIVE COMPOSITIONS OF GARNET

	B1-C	B1-R	B4-C	B4-R	B6-C	B6-R	B33-C	B33-R	B30-C	B0-R	B26-C	B26-R	B11-C	B11-R	B18-C	B18-R	B22-C	B22-R
Oxide weight percents:																		
SiO_2	37.25	37.14	37.59	36.58	37.27	37.52	36.78	36.75	37.38	37.02	37.44	36.85	36.48	37.17	37.08	36.83	37.19	37.13
Al_2O_3	21.21	21.89	21.99	21.19	21.42	21.38	20.91	20.89	21.35	21.09	21.42	21.35	21.53	21.52	21.11	20.84	21.01	21.06
FeO	31.17	34.76	32.75	35.98	33.88	36.22	31.20	30.22	30.36	30.70	34.66	35.40	30.20	27.81	34.36	33.43	33.37	32.82
MgO	0.99	3.54	2.04	3.26	2.28	2.57	1.01	0.91	4.49	3.29	3.31	3.05	2.40	1.72	3.21	2.54	2.45	1.99
MnO	5.32	1.57	4.49	1.14	3.09	0.73	8.40	9.40	3.75	5.07	1.87	2.08	8.54	11.34	3.41	5.52	5.25	6.88
CaO	5.19	1.36	1.87	1.02	3.25	2.54	2.04	1.97	2.18	1.86	1.52	1.02	1.03	1.21	1.10	0.96	0.98	1.06
Σ	101.13	100.26	100.73	99.17	101.19	100.96	100.34	100.14	99.51	99.03	100.22	99.75	100.18	100.77	100.27	100.12	100.25	100.94
Formulas based on Σ(oxygen) / formula = 12:																		
Si	2.988	2.969	3.001	2.973	2.977	2.995	2.994	2.997	2.988	2.998	2.997	2.979	2.954	2.992	2.985	2.987	3.003	2.993
Al	2.006	2.063	2.070	2.030	2.017	2.012	2.006	2.008	2.012	2.013	2.022	2.034	2.054	2.041	2.003	1.993	2.000	2.001
Σ	4.994	5.032	5.071	5.003	4.994	5.007	5.000	5.005	5.000	5.011	5.019	5.013	5.008	5.033	4.988	4.980	5.003	4.994
Fe	2.091	2.324	2.187	2.446	2.263	2.418	2.124	2.061	2.030	2.079	2.321	2.393	2.045	1.871	2.313	2.267	2.254	2.212
Mg	0.118	0.422	0.243	0.395	0.271	0.306	0.123	0.111	0.535	0.397	0.395	0.367	0.290	0.206	0.385	0.307	0.295	0.239
Mn	0.361	0.106	0.304	0.078	0.209	0.049	0.579	0.649	0.254	0.348	0.127	0.142	0.586	0.773	0.233	0.379	0.359	0.470
Ca	0.446	0.116	0.160	0.089	0.278	0.217	0.178	0.172	0.187	0.161	0.130	0.088	0.089	0.105	0.095	0.083	0.085	0.092
Σ	3.017	2.968	2.893	3.008	3.022	2.991	3.003	2.993	3.005	2.985	2.973	2.991	3.010	2.955	3.026	3.037	2.993	3.013
Mole fractions almandine (ALM), pyrope (PYP), spessartine (SPS), and grossular (GRS):																		
ALM	0.693	0.783	0.756	0.813	0.749	0.809	0.707	0.689	0.675	0.696	0.781	0.800	0.679	0.633	0.765	0.747	0.753	0.734
PYP	0.039	0.142	0.084	0.131	0.090	0.102	0.041	0.037	0.178	0.133	0.133	0.123	0.096	0.070	0.127	0.101	0.099	0.079
SPS	0.120	0.036	0.105	0.026	0.069	0.017	0.193	0.217	0.084	0.116	0.043	0.048	0.195	0.262	0.077	0.125	0.120	0.156
GRS	0.148	0.039	0.055	0.030	0.092	0.073	0.059	0.058	0.062	0.054	0.044	0.030	0.030	0.036	0.031	0.027	0.028	0.030

Abbreviations: Analyses of garnet cores (-C) and associated rims (-R). Analytical Details: Beam current in Faraday cup = 15 nA. Standards: Si, Al, Fe – natural almandine; Mn – natural high-Mn hortonolite; Mg, Ca – natural garnet, Roberts Victor mine, South Africa.

neutrality. Each reported composition represents the average of at least three closely spaced individual analyses on individual grains. Details of analytical procedures for individual minerals are given in footnotes in Tables 2–7.

Garnet

Microprobe analytical profiles were made across representative garnet grains from 10 samples across the study area (Table 2, Fig. 5). All garnet grains exhibit significant compositional zoning, and most were found to have relatively simple compositional variations from center to rim. Even the small, anhedral grains of garnet from the higher structural levels have concentric patterns of zoning.

Representative compositions from cores and rims used in thermobarometric calculations are listed in Table 2. Garnet grains from the LSL, especially from staurolite-bearing samples, have a rim enriched in almandine and pyrope and depleted in spessartine and grossular relative to the core (Fig. 5). Garnet from the HSL are small (<1 mm) and weakly zoned; the grains have a rim depleted in pyrope and commonly almandine, and enriched in spessartine, relative to the core (Fig. 5).

The presence of zoning in the garnet in the LSL, in part due to depletion of manganese from the matrix during growth of the garnet (Hollister 1966), suggests that these garnet grains have never been heated much above 600°C (Woodsworth 1977, Yardley 1977, Tracy 1982).

Biotite

Textural observations suggest that several distinct generations of biotite are present in some samples. Representative compositions of biotite adjacent to and included in garnet, in the matrix, and in pressure shadows near garnet are listed in Table 3. In all cases described in Table 3, the biotite coexists with garnet and sillimanite.

Biotite in the matrix is compositionally distinct from biotite in pressure shadows or adjacent to garnet in nearly all samples, but there is no systematic compositional trend between different generations across the field area. Biotite inclusions in garnet are enriched in annite relative to matrix biotite in the LSL samples. We were able to obtain only a few compositions of biotite included in the small grains of garnet of the HSL. Dense intergrowths of fibrolite in some biotite from the LSL prevented acquisition of quantitative analyses of these biotite grains.

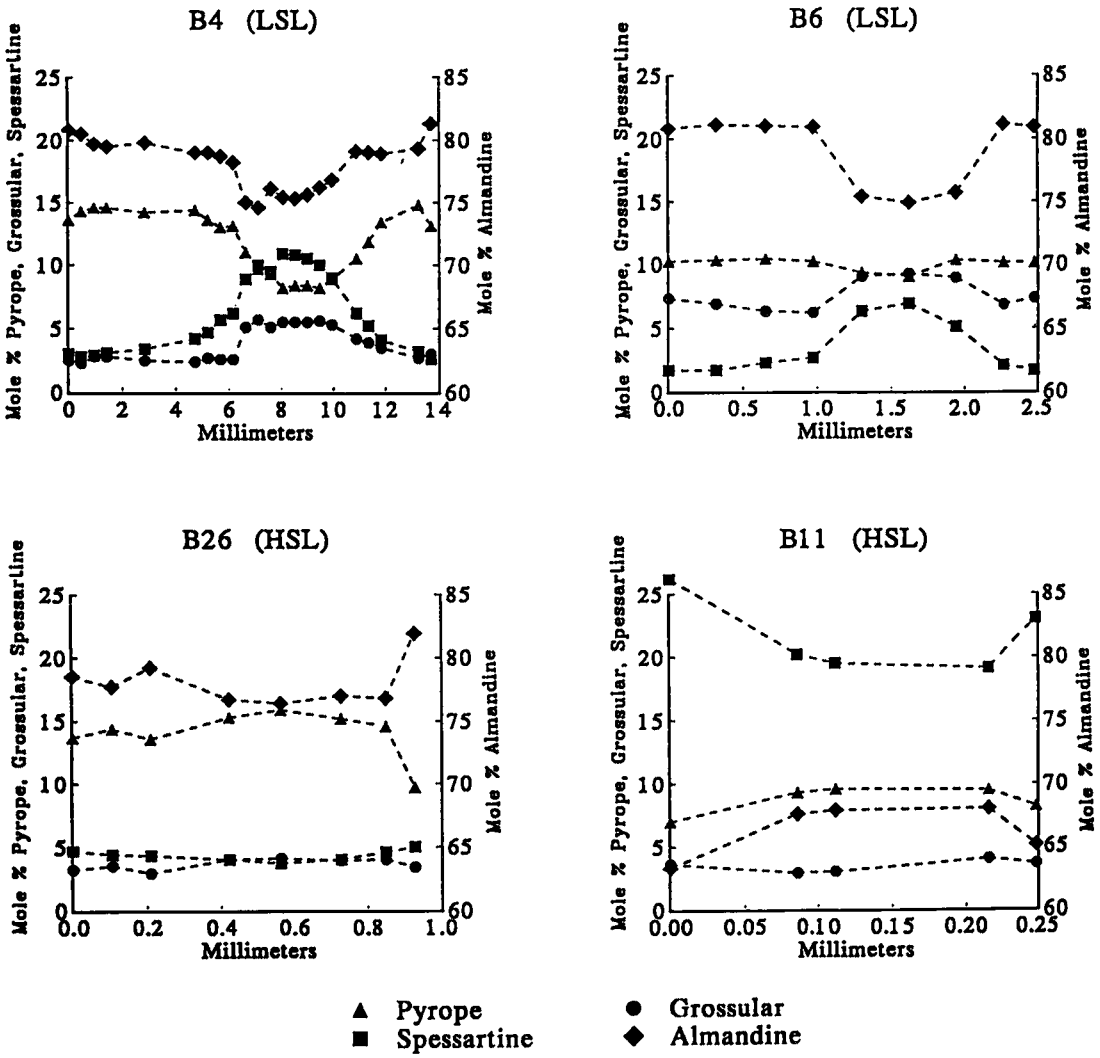

FIG. 5. Representative compositional profiles for garnet from the lower and higher structural levels.

Plagioclase

Plagioclase rims are significantly enriched in calcium relative to cores in the LSL, whereas the opposite trend occurs in the HSL (Table 4). Inclusions of plagioclase in garnet in the LSL are more calcic than the plagioclase in the matrix. Matrix plagioclase in some samples from the HSL contains minor amounts of exsolved alkali feldspar blebs, and some grains of matrix plagioclase have anomalously high values of anorthite. The plagioclase crystals analyzed do not show exsolution features.

Cordierite

The mole fraction of iron is highest in cordierite from the upper part of the HSL and decreases down through the HSL (Table 5). The partition coefficient for Fe relative to Mg in cordierite relative to garnet also decreases from the upper part of the HSL down through structurally lower samples, indicating that variation in cordierite composition is not due solely to variations in bulk composition (assuming ideality). Cordierite is not compositionally zoned, and no significant compositional variation exists within individual samples or

TABLE 3. REPRESENTATIVE COMPOSITIONS OF BIOTITE

Oxide weight percents:

	B1 MTX	B1 PX	B1 INCL	B4 MTX	B4 PS	B6 GRT	B6 PSEUD	B33 MTX	B33 GRT	B33 INCL	B30 MTX	B30 PS	B30 INCL	B26 MTX	B26 GRT	B11 MTX	B11 GRT	B18 MTX	B18 GRT	B22 MTX	B22 GRT
SiO_2	35.64	35.92	36.24	35.98	36.04	34.56	35.23	35.18	33.72	33.80	35.38	35.19	35.71	33.20	34.41	34.89	34.63	34.44	33.99	34.16	34.49
Al_2O_3	19.04	19.56	19.62	19.30	19.94	20.87	20.02	18.35	18.68	18.05	18.99	19.79	19.01	19.54	18.47	20.01	20.18	18.74	19.88	20.04	20.32
TiO_2	3.08	3.30	3.33	2.67	2.13	1.63	2.00	3.85	3.11	3.72	4.34	3.01	3.63	4.04	5.06	3.05	2.00	2.71	2.28	2.53	1.49
FeO	20.05	19.13	19.96	19.92	19.72	21.08	21.23	24.33	24.08	23.45	17.62	17.94	16.93	21.47	20.61	19.69	19.88	19.90	20.30	20.54	21.14
MgO	9.02	9.21	9.05	8.93	9.67	7.40	7.75	4.42	4.67	5.22	8.90	8.60	10.71	7.51	7.04	6.94	7.56	7.89	7.62	6.85	7.17
MnO	0.07	0.07	0.04	0.03	0.06	0.07	0.04	0.39	0.31	0.25	0.16	0.24	0.11	0.13	0.14	0.46	0.44	0.59	0.26	0.34	0.26
CaO	0.00	0.03	0.04	0.03	0.05	0.02	0.05	0.03	0.05	0.05	0.02	0.02	0.07	0.02	0.03	0.02	0.03	0.01	0.07	0.02	0.06
Na_2O	0.18	0.25	0.22	0.38	0.32	0.13	0.16	0.08	0.08	0.19	0.15	0.13	0.17	0.14	0.20	0.11	0.10	0.10	0.16	0.17	0.17
K_2O	9.14	9.13	8.46	8.63	8.28	9.20	8.74	9.46	9.52	9.23	9.28	9.27	9.05	9.16	9.12	9.49	9.51	9.63	9.44	9.54	9.39
Σ	96.22	96.60	96.96	95.87	96.21	94.96	95.22	96.09	94.22	93.96	94.84	94.19	95.39	95.21	95.08	94.66	94.33	94.01	94.00	94.19	94.49
Formulas based on Σ(oxygen)/formula = 11:																					
Si	2.688	2.683	2.693	2.711	2.694	2.655	2.691	2.725	2.674	2.676	2.682	2.688	2.677	2.567	2.647	2.681	2.675	2.682	2.645	2.655	2.673
Al	1.312	1.317	1.307	1.289	1.306	1.345	1.309	1.275	1.326	1.324	1.318	1.312	1.323	1.433	1.353	1.319	1.325	1.318	1.355	1.345	1.327
Σ	4.000	4.000	4.000	4.000	4.000	4.000	4.000	4.000	4.000	4.000	4.000	4.000	4.000	4.000	4.000	4.000	4.000	4.000	4.000	4.000	4.000
Al	0.381	0.405	0.411	0.425	0.452	0.544	0.494	0.401	0.420	0.361	0.380	0.471	0.357	0.347	0.322	0.494	0.512	0.403	0.468	0.492	0.529
Ti	0.175	0.185	0.186	0.151	0.120	0.094	0.115	0.224	0.185	0.225	0.247	0.173	0.205	0.235	0.293	0.176	0.116	0.159	0.133	0.148	0.087
Mg	1.014	1.025	1.002	1.003	1.077	0.847	0.882	0.510	0.552	0.616	1.006	0.979	1.197	0.865	0.807	0.795	0.870	0.916	0.884	0.794	0.828
Fe	1.265	1.195	1.240	1.255	1.233	1.354	1.356	1.576	1.597	1.553	1.117	1.146	1.062	1.388	1.326	1.266	1.284	1.296	1.321	1.335	1.370
Mn	0.004	0.004	0.003	0.002	0.004	0.005	0.003	0.026	0.021	0.017	0.010	0.016	0.007	0.009	0.009	0.030	0.029	0.039	0.017	0.022	0.017
Σ	2.838	2.815	2.842	2.836	2.885	2.844	2.850	2.737	2.775	2.772	2.760	2.785	2.827	2.844	2.757	2.761	2.812	2.812	2.824	2.791	2.831
Ca	0.000	0.002	0.003	0.002	0.004	0.002	0.004	0.002	0.004	0.004	0.002	0.002	0.006	0.002	0.002	0.002	0.002	0.001	0.006	0.002	0.005
Na	0.026	0.036	0.032	0.056	0.046	0.019	0.024	0.012	0.012	0.029	0.022	0.019	0.025	0.021	0.030	0.016	0.015	0.015	0.024	0.026	0.026
K	0.879	0.870	0.802	0.829	0.790	0.902	0.852	0.935	0.963	0.932	0.898	0.903	0.866	0.903	0.895	0.930	0.937	0.957	0.937	0.946	0.928
Σ	0.906	0.909	0.837	0.887	0.840	0.923	0.880	0.949	0.980	0.966	0.921	0.924	0.896	0.926	0.927	0.948	0.954	0.973	0.967	0.973	0.959

Abbreviations: MTX -- biotite from the matrix not near any garnet, PS -- biotite from a pressure shadow touching a garnet, INCL -- biotite inclusion within a garnet, GRT -- biotite adjacent to a garnet but not in any obvious pressure shadow, and PSEUD -- biotite in a pseudomorph after staurolite. Analytical Details: Beam current in Faraday cup = 10 nA. Standards: Si, Al, Ti, Mg, Fe, Ca, Na -- Kakanui hornblende, K -- natural orthoclase, Mn -- natural high-Mn hortonolite.

TABLE 4. REPRESENTATIVE COMPOSITIONS OF PLAGIOCLASE

Oxide Weight Percents:

	B1-C	B1-R	B1-I	B4	B6	B33	B30	B11	B18-C	B18-R	B22-C	B22-R
SiO_2	63.64	62.39	58.50	64.46	58.17	61.43	56.96	60.90	60.82	60.85	60.31	61.33
Al_2O_3	21.95	22.30	25.07	21.11	25.48	24.54	27.00	23.49	23.54	22.55	24.17	23.52
TiO_2	0.01	0.00	0.03	0.00	0.02	0.00	0.01	0.02	0.00	0.00	0.01	0.00
FeO	0.01	0.01	0.22	0.03	0.07	0.01	0.03	0.05	0.02	0.16	0.01	0.06
MgO	0.00	0.00	0.00	0.00	0.00	0.02	0.00	0.00	0.00	0.00	0.01	0.00
CaO	3.62	4.16	7.65	2.70	8.18	5.49	8.58	5.58	5.32	4.87	5.77	4.99
Na_2O	10.05	9.48	7.42	10.33	7.15	8.07	6.20	8.52	8.17	8.61	8.03	8.68
K_2O	0.15	0.12	0.23	0.11	0.12	0.24	0.21	0.21	0.33	0.37	0.34	0.26
Σ	99.33	98.46	99.12	98.74	99.19	99.80	98.98	98.77	98.20	97.41	98.65	98.83

Formulas based on Σ(Al + Si) / formula = 4:

Si	2.844	2.814	2.657	2.886	2.638	2.719	2.566	2.750	2.747	2.784	2.717	2.755
Al	1.156	1.186	1.343	1.114	1.362	1.281	1.434	1.250	1.253	1.216	1.283	1.245
Σ	4.000	4.000	4.000	4.000	4.000	4.000	4.000	4.000	4.000	4.000	4.000	4.000
Ti	0.000	0.000	0.001	0.000	0.001	0.000	0.000	0.001	0.000	0.000	0.000	0.000
Fe	0.000	0.000	0.008	0.001	0.003	0.000	0.001	0.002	0.001	0.006	0.000	0.002
Ca	0.169	0.201	0.372	0.130	0.397	0.260	0.414	0.270	0.257	0.239	0.278	0.240
Na	0.871	0.829	0.654	0.897	0.629	0.693	0.542	0.746	0.715	0.764	0.701	0.756
K	0.009	0.007	0.013	0.006	0.007	0.014	0.012	0.012	0.019	0.022	0.020	0.014
Σ	1.049	1.037	1.049	1.034	1.036	0.967	0.969	1.030	0.993	1.030	1.001	1.013

Mole fractions albite (AB), orthoclase (OR), and anorthite (AN):

AB	0.831	0.799	0.629	0.868	0.609	0.717	0.560	0.726	0.721	0.746	0.702	0.748
OR	0.008	0.007	0.013	0.006	0.007	0.014	0.012	0.012	0.019	0.021	0.020	0.014
AN	0.161	0.194	0.358	0.125	0.385	0.269	0.428	0.263	0.260	0.233	0.279	0.238

Abbreviations: Plagioclase cores (-C) and rims (-R) in samples containing compositionally zoned crystals. Plagioclase occurring as inclusions in garnet (-I). Analytical Details: Beam current in Faraday cup = 10 nA, raster beam over 5 square micron area during analysis. Standards: Si, Al, Ca – natural laboradorite, Lake County, OR; Fe, Mg, Ti, K – Kakanui hornblende; Na – natural albite.

between texturally distinct generations of cordierite.

Staurolite

Staurolite (Table 6) is weakly zoned in most samples. Zinc is slightly enriched in the core relative to the rim. Staurolite is probably not present in samples B1 and 2 because the Ca and Mn content of the garnet indicates that these samples may plot in a compositional field where staurolite is not stable.

Muscovite and K-feldspar

Representative compositions of muscovite are given in Table 7. Muscovite composition does not vary systematically with structural position in the study area. One sample of K-feldspar was X-rayed and found to be orthoclase.

Thermometry and Barometry

Many of the aluminosilicate-bearing rocks contain low-variance assemblages, and one or more minerals in each preserve compositional zoning. These samples are appropriate candidates for the application of several geothermometers and geobarometers.

Garnet–biotite geothermometry

Garnet and biotite compositional data for nine samples from across the study area were used in the application of the geothermometer models of Ferry & Spear (1978), Perchuk & Lavrent'eva (1983), Ganguly & Saxena (1984), and Hodges & Spear (1982). Data for garnet cores and rims were combined with data for biotite from the matrix, from pressure shadows of the garnet, from inclusions in the garnet and from adjacent to the garnet.

Temperatures calculated for pressures between 2 and 10 kbar for all samples are relatively insensitive to pressure. The range in temperatures (Table 8) calculated by the various models is large, but trends in temperature are similar. Random errors in calculated temperatures for the experimentally calibrated models are on the order of ±50°C (Ferry & Spear 1978, Hodges & Crowley 1985). The choice of garnet–biotite model is somewhat arbitrary, but is less critical in considering relative variations, which is the objective of this study, than it is for determining absolute temperatures and pressures.

For purposes of discussion, we use the temperatures based on the model of Ganguly & Saxena. This choice is made because the results are most consistent with the temperatures inferred from the reactions and because these temperatures lead to geologically reasonable and systematic variations in pressure in the barometric calculations.

In nearly all cases, model temperatures derived from garnet cores and biotite inclusions are close to those from garnet cores and matrix biotite, but are significantly different from temperatures obtained from garnet cores and adjacent or pressure-shadow biotite. The textural observations suggest that the scale of equilibration during postkinematic reactions may have been considerably less than the distance across a standard petrographic thin section. For this reason, core temperatures were calculated using biotite inclusions wherever possible; otherwise, matrix biotite far from garnet was used. Rim temperatures were calculated using adjacent biotite or pressure-shadow biotite (or both) in contact with the analyzed garnet rim.

Examination of the representative temperatures (Tables 8, 9) yields the following generalizations. Samples from the LSL show a large increase in model temperature from core to rim, whereas samples from the HSL show small decreases. Based on the garnet–biotite thermometry, temperature increased in the LSL and decreased slightly in the HSL during the garnet growth, which followed deformation. Furthermore, the earliest model temperatures in the LSL are considerably lower than the earliest recorded model temperatures in

TABLE 5. REPRESENTATIVE COMPOSITIONS OF CORDIERITE

Oxide Weight Percents:

	B30	B28	B26	B18
SiO_2	49.78	47.82	47.14	47.23
Al_2O_3	32.95	33.62	32.54	32.79
FeO	8.19	9.81	9.83	10.24
MgO	7.99	7.41	7.05	6.44
MnO	0.35	0.56	0.16	0.50
CaO	0.03	0.05	0.06	0.05
Na_2O	0.11	0.00	0.16	0.23
Σ	99.40	99.26	96.94	97.48

Formulas, Σ(oxygen)/formula=18:

Si	4.971	4.923	4.965	4.963
Al	4.040	4.079	4.040	4.061
Σ	9.011	9.002	9.005	9.024
Fe	0.713	0.845	0.866	0.900
Mg	1.239	1.137	1.107	1.009
Mn	0.031	0.049	0.014	0.045
Ca	0.003	0.006	0.007	0.006
Na	0.022	0.000	0.033	0.047
Σ	2.008	2.037	2.027	2.007
X(Fe)	0.355	0.415	0.427	0.448
X(Mg)	0.617	0.558	0.546	0.503

Analytical Details: Beam current in Faraday cup = 15 nA. Standards: Si, Al, Ca – natural labradorite, Lake Co., OR; Ti, Fe, Na – Kakanui hornblende; Mg – synthetic forsterite.

TABLE 6. REPRESENTATIVE COMPOSITIONS OF STAUROLITE

Oxide Weight Percents:

	B4 CORE	B4 EDGE	B6 CORE	B6 EDGE	B7 CORE	B7 EDGE
SiO_2	28.03	28.24	28.08	28.08	27.51	27.37
Al_2O_3	55.02	54.55	55.42	55.24	54.89	55.48
TiO_2	0.76	0.76	0.75	0.69	0.64	0.68
FeO	13.84	13.45	13.22	12.61	13.97	14.90
MgO	1.49	1.50	1.28	1.08	1.27	1.18
ZnO	0.52	0.31	0.80	0.68	0.10	0.05
MnO	0.12	0.10	0.03	0.04	0.14	0.22
Σ	99.78	98.91	99.58	98.42	98.52	99.88

Formulas based on Σ(oxygen) / formula = 47, exclusive of H_2O:

Si	7.805	7.906	7.815	7.876	7.751	7.643
Al	0.195	0.094	0.185	0.124	0.249	0.357
Σ	8.000	8.000	8.000	8.000	8.000	8.000
Al	17.868	17.910	17.999	18.141	17.983	17.907
Ti	0.159	0.160	0.157	0.146	0.136	0.143
Fe	3.223	3.149	3.077	2.958	3.292	3.480
Mg	0.618	0.626	0.531	0.451	0.533	0.491
Mn	0.028	0.024	0.007	0.010	0.033	0.052
Zn	0.107	0.064	0.164	0.141	0.021	0.010
Σ	22.003	21.933	21.935	21.847	21.998	22.083

Note: Staurolite occurs only as inclusions in sample B7. Analytical Details: Beam current in Faraday cup = 15 nA. Standards: Si, Al – natural kyanite; Zn – natural gahnite; Fe, Mg, Ti – Kakanui hornblende; Mn – natural high-Mn hortonolite.

the HSL. These conclusions are largely independent of which garnet – biotite geothermometer is selected, and they are the same as those arrived at by considering the reaction textures discussed above. A probable explanation for the smaller changes in model temperature in the HSL than the LSL is that the high temperatures of the HSL and the small size of garnet grains resulted in volume diffusion throughout the garnet grains (Spear 1991) of the HSL.

Garnet – cordierite geothermometry

Garnet and cordierite compositions in three samples from the HSL were used to calculate temperatures using the models of Perchuk & Lavrent'eva (1983) and Bhattacharya *et al.* (1988).

TABLE 7. REPRESENTATIVE COMPOSITIONS OF MUSCOVITE

Oxide Weight Percents:

	B1	B4	B6	B33	B30
SiO_2	46.60	46.14	46.43	46.04	45.75
Al_2O_3	33.76	34.59	34.94	34.53	36.04
TiO_2	1.11	0.83	0.90	1.35	0.03
FeO	1.18	1.07	1.11	1.50	1.05
MgO	0.90	0.64	0.59	0.74	0.63
MnO	0.03	0.04	0.03	0.02	0.04
CaO	0.03	0.03	0.04	0.01	0.02
Na_2O	0.69	1.12	0.67	0.24	0.22
K_2O	9.05	8.17	9.19	8.29	9.80
Σ	93.35	92.63	93.90	92.72	93.58

Formulas based on Σ(oxygen)/formula=11:

Si	3.137	3.115	3.107	3.105	3.076
Al	0.863	0.885	0.893	0.895	0.924
Σ	4.000	4.000	4.000	4.000	4.000
Al	1.817	1.869	1.863	1.851	1.932
Ti	0.056	0.042	0.045	0.068	0.002
Mg	0.090	0.064	0.059	0.074	0.063
Fe	0.066	0.060	0.062	0.085	0.059
Mn	0.002	0.002	0.002	0.001	0.002
Σ	2.031	2.038	2.031	2.080	2.058
Ca	0.002	0.002	0.003	0.001	0.001
Na	0.090	0.147	0.087	0.031	0.029
K	0.777	0.704	0.785	0.713	0.841
Σ	0.870	0.853	0.874	0.746	0.871

Analytical Details: Beam current in Faraday cup = 10 nA, raster beam over 5 square micron area during analysis. Standards: Si, Al, Ca – natural laboradorite, Lake Co, OR; Ti, Mg, Fe, Na – Kakanui hornblende; K – natural orthoclase; Mn – natural high-Mn hortonolite.

TABLE 8. REPRESENTATIVE TEMPERATURE AND PRESSURE RESULTS USING VARIOUS MODELS FOR GARNET-BIOTITE THERMOMETRY AND GARNET-PLAGIOCLASE-ALUMINOSILICATE-QUARTZ BAROMETRY

TEMPERATURES

Sample B1

Garnet Core + Matrix Biotite:

Pressure	F&S	P&L	G&S	H&S
3000	343	458	423	393
5000	349	447	428	398
7000	354	436	434	404
9000	360	426	439	409

Garnet Rim + Adjacent Biotite:

Pressure	F&S	P&L	G&S	H&S
3000	633	639	587	649
5000	642	626	595	658
7000	650	613	603	666
9000	658	600	611	674

Sample B33

Garnet Core + Matrix Biotite:

Pressure	F&S	P&L	G&S	H&S
3000	574	607	679	598
5000	582	594	687	606
7000	590	582	694	613
9000	597	569	702	621

Garnet Rim + Adjacent Biotite:

Pressure	F&S	P&L	G&S	H&S
3000	528	580	634	550
5000	535	567	642	558
7000	542	555	649	565
9000	549	543	656	572

Sample B18

Garnet Core + Matrix Biotite:

Pressure	F&S	P&L	G&S	H&S
3000	676	662	652	689
5000	685	648	661	698
7000	693	635	669	706
9000	702	621	677	715

Garnet Rim + Adjacent Biotite:

Pressure	F&S	P&L	G&S	H&S
3000	617	630	633	628
5000	625	617	641	636
7000	633	604	649	644
9000	641	591	657	652

PRESSURES

Garnet Core + Plagioclase Core:

Temp.	K&N	N&H	Gt&St	Ghent
300	5225	4149	4285	4281
600	11870	11482	11074	11491
900	18516	18816	17862	18701

Garnet Rim + Plagioclase Rim:

Temp.	K&N	N&H	Gt&St	Ghent
300	1067	978	228	991
600	5141	5800	4429	6479
900	9215	10621	8631	11966

Garnet Core + Ave. Plagioclase:

Temp.	K&N	N&H	Gt&St	Ghent
300	784	921	0	1496
600	4818	5792	4000	6979
900	8819	10663	8197	12463

Garnet Rim + Ave. Plagioclase:

Temp.	K&N	N&H	Gt&St	Ghent
300	711	854	0	1451
600	4731	5693	3916	6911
900	8718	10533	8098	12371

Garnet Core + Plagioclase Core:

Temp.	K&N	N&H	Gt&St	Ghent
300	0	0	0	0
600	2683	3723	1885	4540
900	5641	7606	5033	9186

Garnet Rim + Plagioclase Rim:

Temp.	K&N	N&H	Gt&St	Ghent
300	0	0	0	0
600	2263	3503	1466	4426
900	5219	7372	4612	9032

Abbreviations: F&S Ferry & Spear (1978), P&L Perchuk & Lavrent'eva (1983), G&S Ganguly & Saxena (1984), H&S Hodges & Spear (1982), K&N Koziol & Newton (1988), Newton & Haselton (1981), Gt&St Ghent & Stout (1981), and Ghent (1976). Estimates of errors are discussed in the text.

TABLE 9. PRESSURES CALCULATED FROM GARNET CORE AND GARNET RIM COMPOSITIONS USING SEVERAL MODELS

	CORES					RIMS				
	T(core)	K&N	N&H	Gt&St	Ghent	T(rim)	K&N	N&H	Gt&St	Ghent
B1	430	8.1	7.3	7.2	7.4	610	5.3	6.0	4.6	6.7
B4	530	6.7	7.4	5.8	7.6	590	5.3	6.4	4.5	6.9
B6	620	6.7	7.1	5.8	7.4	630	5.4	6.1	4.6	6.8
B33	660	5.6	6.8	4.8	7.9	610	4.9	5.8	4.0	6.9
B30	600	4.8	4.9	4.0	5.4	640	4.0	4.7	3.2	5.6
B11	700	3.3	4.6	2.6	6.2	625	3.2	4.3	2.5	5.6
B18	650	3.2	4.4	2.4	5.6	610	2.4	3.6	1.6	4.8
B22	670	2.3	3.8	1.6	5.3	620	2.6	4.0	1.8	5.3

Abbreviations are given in the footnote to Table 8. Error estimates are discussed in the text.

TABLE 10. CORDIERITE TEMPERATURES COMPARED TO GARNET-BIOTITE TEMPERATURES

	Garnet Core + Cordierite				Garnet Rim + Cordierite			
	P&L	B	F&S	G&S	P&L	B	F&S	G&S
B26	610	700	(750)	(710)	580	680	(710)	(680)
B30	650	760	(670)	(600)	560	700	(650)	(640)
B18	640	720	(680)	(650)	580	680	(600)	(610)

Abbreviation: B Bhattacharya et al. (1988). The remaining abbreviations are given in footnote to Table 8. Garnet – biotite temperatures are shown in parentheses. Estimates of errors are discussed in the text.

Garnet rims were considered to be in equilibrium with the adjacent cordierite. As in garnet–biotite calculations, the temperatures are relatively insensitive to pressure, and there are large differences between temperatures calculated by different models (Table 10). Random errors in calculated temperatures in these models are expected to be at least ±65°C in this temperature range. The Ganguly & Saxena garnet–biotite temperatures are in closest agreement with the Bhattacharya *et al.* (1988) garnet–cordierite temperatures. Garnet–biotite and garnet–cordierite temperatures are significantly different, but the assemblages may not have been coeval, or equilibrium may not have been achieved.

Garnet – plagioclase – aluminosilicate – quartz geobarometry

Pressures were calculated for garnet and plagioclase data for eight samples with the models of Koziol & Newton (1988), Newton & Haselton (1981), Ganguly & Saxena (1984), and Ghent (1976) (Table 10). Garnet cores are considered to have equilibrated with plagioclase inclusions or with plagioclase in the matrix, and garnet rims are considered to have equilibrated with adjacent plagioclase. In samples with significantly zoned plagioclase, garnet and plagioclase cores are used to determine the pressure at which garnet began to grow, and garnet and plagioclase rims are used to determine pressure at the end of garnet growth.

Calculated pressures are strongly dependent on temperature. Temperatures based on garnet–biotite thermometry were used to calculate pressures (Tables 8, 9). Expected errors in calculated pressures using these models in this P–T range are on the order of ±1 kbar (Hodges & Crowley 1985). As with the geothermometers, different models produce significantly different pressures. However, systematic trends are defined by core and rim calculations for individual samples, especially when the pressures are based on the Ganguly & Saxena garnet–biotite temperature estimates. Because they have fewer internal inconsistencies, the Newton & Haselton pressure results are used for the purpose of comparison. Rim pressures are 2 – 3 kbar lower than core pressures in the LSL, and 1 – 2 kbar lower than core pressures in the HSL. Based on the rims, a pressure difference of approximately 2.2 kbar is recorded between the HSL and LSL. This estimate corresponds to 9 km of structural relief across the area, which is about what would be estimated from the cross-sections of Gansser (1983).

The cores of large (3–15 mm), zoned grains of garnet from the LSL have probably recorded a longer history, including early, low-temperature, high-pressure metamorphism. Any early-pressure history of the HSL, with the exception of the one relict grain of kyanite (Fig. 3h), has been obliterated by reaction and by diffusion (Spear 1991) due to the high temperatures of metamorphism reached in the HSL. Overall, the barometric results are consistent with an interpretation of uplift of the entire study area as a hot package.

Summary of P–T Paths

The apparent P–T path of the LSL samples (Fig. 4a) indicates an increase of temperature during growth of the garnet; the unzoned rims of the garnet probably grew during the reaction that consumed staurolite. The LSL probably experienced pressures of about 7 kbar prior to an episode of deformation. The reaction that consumed staurolite proceeded at a model pressure of about 6 kbar as a result of heating to about 640°C.

The mineral compositions from the HSL do not record the decompression inferred from the preserved reaction textures (Fig. 4b). Our data indicate that the P–T conditions of last equilibration were about 4 kbar and 630°C. In contrast to the LSL, the compositional zoning of the garnet rims and the homogeneous compositions of the garnet cores suggest that these conditions were achieved during cooling from temperatures of at least 650°C (probably near 700°C); the hercynite-bearing symplectite implies a maximum temperature of over 700°C.

Conclusions

The metamorphic features of the upper portion of the Tibetan slab in Bhutan define two geographic subdivisions based on distinctive textures and mineral assemblages: the higher structural levels (HSL) and the lower structural levels (LSL).

The LSL is within the central portion of the Tibetan slab, well above the Main Central thrust; it structurally and topographically underlies the HSL. In the LSL, a penetrative fabric postdates mineral assemblages formed at conditions of about 480°C – 500°C, and about 7 kbar. The penetrative fabric mostly predates mineral assembages that formed at up to about 640°C and 6 kbar.

The HSL contains mineral assemblages with model conditions of 4 kbar and 630°C. Based on the mineral assemblages and patterns of zoning in garnet, the HSL cooled from temperatures of at least 650°C – 700°C. The occurrence of kyanite relics and the textures indicative of reactions that

commenced during decompression imply that the pressure of the HSL dropped to 4 kbar from a higher, unrecorded pressure. Late fibrolite and muscovite in the HSL can be attributed to further reactions during cooling and decompression.

The metamorphic history of the LSL could have begun at any time when there was a normal geothermal gradient, in this case about 20°C/km. The assemblages of the LSL were later affected by the penetrative deformation, which could correlate with collision of India with Asia. The penetrative fabric in the LSL was overprinted by metamorphic assemblages indicating temperatures in excess of 600°C and at a pressure of about 6 kbar, indicating that a thermal perturbation was accompanied by about 5 km of exhumation. There are no recognizable magmatic bodies that could be a heat source within or structurally below the LSL, which is itself in the hanging wall of the Main Central thrust. However, the high temperatures indicated for the metamorphism of the HSL suggest that it could be the heat source.

Two lines of evidence indicate that the country rock of the HSL was already hot when the leucogranites intruded. First, the development of the high-temperature metamorphic assemblages is widespread in the study area, and their occurrence is not restricted to areas proximal to known leucogranite bodies. Second, textural observations demonstrate that reactions [4] and [6], which produced some of the high-temperature assemblages, predate the latest deformation, whereas the leucogranites clearly cross-cut the fabric of the HSL in Bhutan (Gansser 1983).

The temporal relations between reactions and deformation suggest the possible existence of a thrust shear-zone of considerable cumulative displacement between the lower and higher structural levels within the Tibetan slab and above the Main Central thrust. Within Bhutan, the thrust shear-zone includes locality 7 (Fig. 2). This deformation must have occurred at considerable crustal depths, and emplaced "hot rocks onto warm rocks" rather than "hot rocks onto cold rocks".

The proposed thrusting probably predates the last motion on the Main Central thrust because it occurred at a much higher temperature, ~600°C, compared to the greenschist-facies conditions under most of the Main Central thrust in Bhutan. In this interpretation, the upper and lower structural levels would have been brought up subsequently along the Main Central thrust; this would have been at about 15 – 20 Ma ago (Le Fort 1986, Hubbard & Harrison 1989). Later, displacement stepped down to the Main Boundary fault. In our model, we are proposing the existence of a zone of significant displacement that developed earlier than the Main Central thrust as mapped in Bhutan. However, because we have so few constraints on our hypothesized thrust-shear, we cannot exclude an out-of-sequence thrust.

Models have been proposed by others (*e.g.*, Le Fort 1981, Jaupart & Provost 1985, Pinet & Jaupart 1987) to account for the thermal anomaly identified elsewhere in the Tibetan slab and which we have described in Bhutan. Because of the substantial shear-displacement and the evidence for high-temperature decompression of the HSL, we suggest that the primary input of heat into the HSL may have occurred near the base of the crust prior to the thrusting.

Figure 6 illustrates how such a heat source would be consistent with our observations. For purposes of illustration, we assume the initial heating of the hanging wall to be due to underplating of the crust by basaltic magma. The hot spot (Figs. 6a, b) would have created a zone of weak, partially molten rocks within which, during convergence, the shear zone would be initiated, which resulted in emplacement of the hot hanging-wall over the warm footwall (Fig. 6c). This is one way in which heat can be tectonically transported into the middle crust.

The remaining steps in development of the metamorphism and deformation of the Tibetan slab in Bhutan are constrained by petrological and field data. The whole Tibetan slab was uplifted along the Main Central thrust (Fig. 6d) at about 20 Ma, and nearly synchronous normal faulting (Burg *et al.* 1984, Burchfiel & Royden 1985, Herren 1987) removed the overlying Tibetan Series back toward the north (Figs. 6d, e). The resultant drop in lithostatic load led to the high-temperature decompression reactions we described in the higher structural level. The relations involving time – metamorphism – deformation fabric of the leucogranites to the host rocks allow the inference that the leucogranitic magmas were collected from the still partially molten hanging-wall during the tectonic denudation (Fig. 6e).

The formation of the inverted metamorphic gradient within the Tibetan slab, the complex and partially equilibrated assemblages, and the preservation of the textures produced as a result of high-temperature decompression reactions in the higher structural levels all point to an extremely rapid series of heating, deformation, and exhumation events. However, much more work needs to be done in Bhutan, as well as in the rest of the Himalaya, before the interrelationships of these events are fully understood.

Acknowledgements

This study was made possible by a trek organized

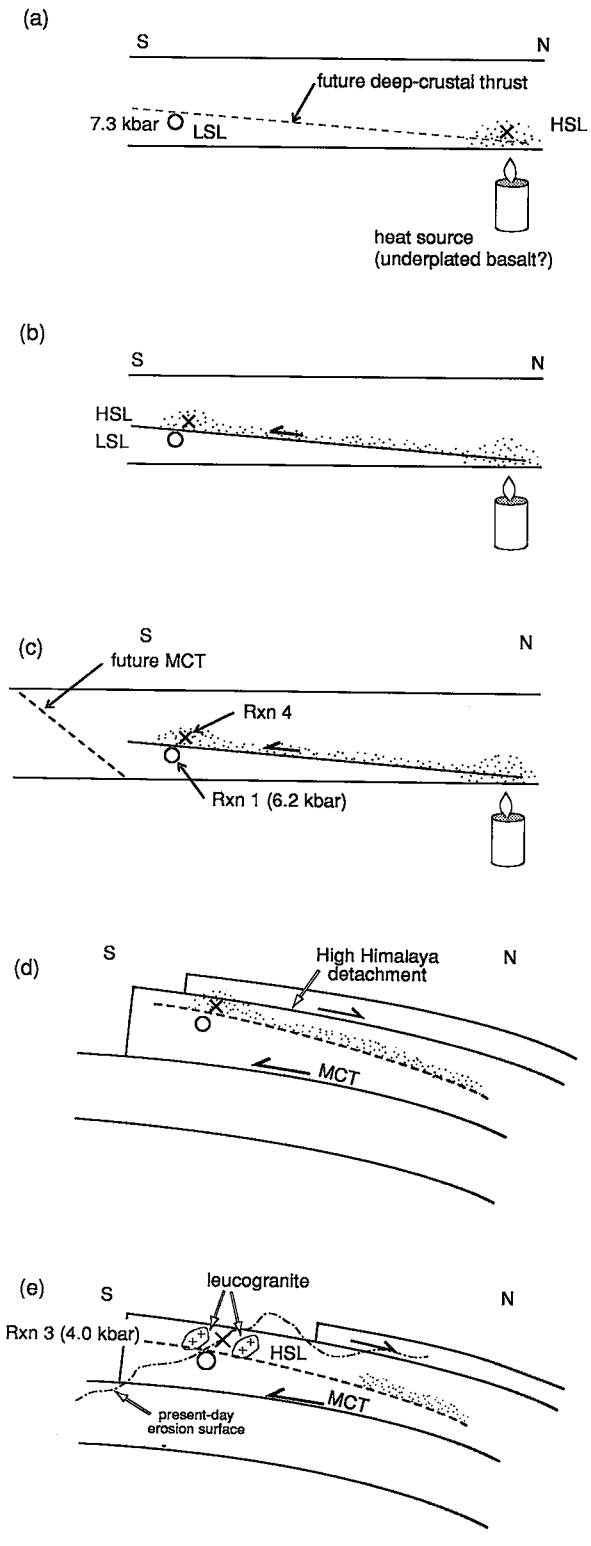

FIG. 6. Schematic tectonic settings for the metamorphism of the upper Tibetan slab in Bhutan. (a) Lower Structural Level (o) is metamorphosed under "normal" thermal conditions near the base of the continental crust (7.3 kbar). The Higher Structural Level (x) is also near the base of the crust, but it is heated by an external source of heat, possibly underplated basaltic magma. The stippled areas represent regions of anatexis. (b) The Higher Structural Level is thrust over the Lower Structural Level. The thrust zone is initiated within the partially melted region in the crust, above the heat source. The stippled area remains partially molten after thrusting. (c) Reaction 1 occurs in the Lower Structural Level at 6.2 kbar owing to heat conducted down from the Higher Structural Level. Dashed line schematically illustrates the site of future Main Central thrust (MCT). (d) Displacement along MCT leads to crustal thickening and removal of some load by normal faulting through the higher part of the Tibetan slab. (e) Following tectonic exhumation, the decompression reactions (*e.g.*, reaction 5) are recorded at 4 kbar, and leucogranitic melt collects from the migmatite as plutons within extension zones formed during normal faulting.

by Charles D. Hollister into the high Himalaya of Bhutan. Because of his experience from two previous expeditions into Bhutan, he was able to lead a small group into areas rarely visited by outsiders. We also were fortunate to have the best of the support personnel that could be provided by the Bhutan Tourist Agency. For the sample collecting, LSH was assisted by his wife Sarah, who also kept him company during the long hours of isolation from the group caused by his taking the time to collect samples and to make structural measurements. Thanks to the perception and understanding of the government authorities in Bhutan, we were allowed to take our samples with us. Thin sections were initially prepared by Toni Willi at ETH, Zurich. LSH is grateful to Rainer Kundig of the ETH for discussions on problems of the geology of the Himalaya. The microprobe work was done at Rutgers University with the financial assistance of the Department of Geological and Geophysical Sciences, Princeton University. The manuscript benefitted substantially from the reviews of K. Hodges and E. Zaleski. We hope this paper is up to the high standards set by Hugh Greenwood, to whom it is dedicated.

REFERENCES

ALLÈGRE, C.J., COURTILLOT, V., TAPPONNIER, P., HIRN, A., MATTAUER, M., COULON, C., JAEGER, J.J., ACHACHE, J., SCHÄRER, U., MARCOUX, J., BURG, J.P., GIRARDEAU, J., ARMIJO, R., GARIÉPY, C., GÖPEL, C., ALLÈGRE, C.J., COURTILLOT, V., TAPPONNIER, P., HIRN, A., MATTAUER, M., COULON, C., JAEGER, J.J., ACHACHE, J., SCHÄRER, U., MARCOUX, J., BURG, J.P., GIRARDEAU, J., ARMIJO, R., GARIÉPY, C., GÖPEL, C., LI TINDONG, XIAO XUCHANG, CHANG CHENFA, LI GUANGQIN, LIN BAOYU, TENG JIWEN, WANG NAIWEN, CHEN GUOMING, HAN TONGLIN, WANG XIBIN, DEN WANMING, SHENG HUAIBIN, CAO YOUGONG, ZHOU JI, QIU HONGRONG, BAO PEISHENG, WANG SONGCHAN, WANG BIXIANG, ZHOU YAOXIU & XU RONGHUA (1984): Structure and evolution of the Himalaya-Tibet orogenic belt. *Nature* **307**, 17-22.

BANERJEE, H., DASGUPTA, S., BHATTACHARYA, P.K. & SURKAR, S.C. (1983): Evolution of the lesser Himalayan metapelites of the Sikkim - Darjeeling region, India, and some related problems. *Neues Jahrb. Mineral. Abh.* **146**, 197-209.

BARNICOAT, A.C. & TRELOAR, P.J. (1989): Himalayan metamorphism - an introduction. *J. Metamorph. Geol.* **7**, 3-8.

BERMAN, R.G. (1988): Internally-consistent thermodynamic data for minerals in the system Na_2O-K_2O-CaO-MgO-FeO-Fe_2O_3-Al_2O_3-SiO_2-TiO_2-H_2O-CO_2. *J. Petrol.* **29**, 445-522.

BHATTACHARYA, A., MAZUMDAR, A.C. & SEN, S.K. (1988): Fe-Mg mixing in cordierite: constraints from natural data and implications for cordierite - garnet geothermometry in granulites. *Am. Mineral.* **73**, 338-344.

BOUCHEZ, J.L. & PECHER, A. (1981): The Himalayan Main Central Thrust pile and its quartz-rich tectonites in central Nepal. *Tectonophys.* **78**, 23-50.

BRUNEL, M. & KIENAST, J.-R. (1986): Etude pétrostructurale des chevauchements ductiles, himalayens sur la traversale de l'Everest - Makalu (Népal oriental). *Can. J. Earth Sci.* **23**, 1117-1137.

BURCHFIEL, B.C. & ROYDEN, L.H. (1985): North-south extension within the convergent Himalayan region. *Geology* **13**, 679-682.

BURG, J.P., BRUNEL, M., GAPAIS, D., CHEN, G.M. & LIU, G.H. (1984): Deformation of leucogranites of the crystalline Main Central sheet in southern Tibet (China). *J. Struct. Geol.* **6**, 535-542.

CHAMBERLAIN, C.P., ZEITLER, P.K. & JAN, M.Q. (1989): The dynamics of the suture between the Kohistan Island arc and the Indian plate in the Himalaya of Pakistan. *J. Metamorph. Geol.* **7**, 135-149.

DEBON, F, LE FORT, P., SHEPPARD, S.M.F. & SONET, J. (1986): The four plutonic belts of the Transhimalaya - Himalaya: a chemical, mineralogical, isotopic, and chronological synthesis along a Tibet - Nepal section. *J. Petrol.* **27**, 219-250.

DENIEL, C., VIDAL, P., FERNANDEZ, A., LE FORT, P. & PEUCAT, J.-J. (1987): Isotopic study of the Manaslu granite (Himalaya, Nepal): inferences on the age and source of Himalayan leucogranites. *Contrib. Mineral. Petrol.* **96**, 78-92.

DIETRICH, V. & GANSSER, A. (1981): The leucogranites of the Bhutan Himalaya (crustal anatexis versus mantle melting). *Schweiz. Mineral. Petrogr. Mitt.* **61**, 177-202.

DUTROW, B.L. & HOLDAWAY, M.J. (1989): Experimental determination of the upper thermal stability of Fe-staurolite + quartz at medium pressures. *J. Petrol.* **30**, 229-248.

FERRARA, G., LOMBARDO, B. & TONARINI, S. (1983): Rb/Sr geochronology of granites and gneisses from the Mount Everest region, Nepal Himalaya. *Geol. Rundschau* **72**, 119-136.

———, ———, ——— & TURI, B. (1985): Miocene anatexis in the Higher Himalayan basement nappes: $^{87}Sr/^{86}Sr$ and $^{18}O/^{16}O$ evidence from the Gophy La leucogranite of Bhutan. *Terra Cognita* **5**(2-3), 228 (abstr.).

FERRY, J.M. & SPEAR, F.S. (1978): Experimental calibration of the partitioning of Fe and Mg between biotite and garnet. *Contrib. Mineral. Petrol.* **66**, 113-117.

FOSTER, C.T., JR. (1977): Mass transfer in sillimanite-bearing pelitic schists near Rangeley, Maine. *Am. Mineral.* **62**, 727-746.

——— (1981): A thermodynamic model of mineral segregations in the lower sillimanite zone near Rangeley, Maine. *Am. Mineral.* **66**, 260-277.

——— (1983): Thermodynamic models of biotite pseudomorphs after staurolite. *Am. Mineral.* **68**, 389-397.

FRANK, W., HOINKES, G., MILLER, C., PURTSCHELLER, F., RICHTER, W. & THÖNI, M. (1973): Relations between metamorphism and orogeny in a typical section of Indian Himalayas. *Tschermaks Mineral. Petrogr. Mitt.* **20**, 303-332.

GANGULY, J. & SAXENA, S.K. (1984): Mixing properties of alumino-silicate garnets: constraints from natural and experimental data and its application to geothermo-barometry. *Am. Mineral.* **69**, 88-97.

GANSSER, A. (1964): *Geology of the Himalayas.* John Wiley, New York.

_____ (1983): *Geology of the Bhutan Himalaya.* Birkhauser Verlag, Basel.

GARIÉPY, C., ALLÈGRE, C.J. & XU RONG-HUA (1985): The Pb-isotope geochemistry of granitoids from the Himalaya–Tibet collision zone: implications for crustal evolution. *Earth Planet. Sci. Lett.* **74**, 220-234.

GHENT, E.D. (1976): Plagioclase – garnet – Al_2SiO_5 – quartz: a potential geobarometer – geothermometer. *Am. Mineral.* **61**, 710-714.

_____ & STOUT, M.Z. (1981): Geobarometry and geothermometry of plagioclase – biotite – garnet – muscovite assemblages. *Contrib. Mineral. Petrol.* **76**, 92-97.

GRANT, J.A. & WEIBLEN, P.W. (1971): Retrograde zoning in garnet near the second sillimanite isograd. *Am. J. Sci.* **270**, 281-296.

GUIDOTTI, C.V. (1974): Transition from staurolite to sillimanite zone, Rangeley quadrangle, Maine. *Geol. Soc. Am. Bull.* **85**, 475-490.

HERREN, E. (1987): Zanskar shear zone: northeast-southwest extension within the Higher Himalayas (Ladakh, India). *Geology* **15**, 409-413.

HODGES, K.V. & CROWLEY, P.D. (1985): Error estimation and empirical geothermobarometry for pelitic systems. *Am. Mineral.* **70**, 702-709.

_____, HUBBARD, M.S. & SILVERBERG, D.S. (1988a): Metamorphic constraints on the thermal evolution of the central Himalayan orogen. *Phil. Trans., Roy. Soc. London* **A326**, 257-280.

_____, LE FORT, P. & PÊCHER, A. (1988b): Possible thermal buffering by crustal anatexis in collisional orogens: thermobarometric evidence from the Nepalese Himalaya. *Geology* **16**, 707-710.

_____, LUX, D., BURCHFIEL, B.C., ROYDEN, L.H., CHEN, Z., DENG, C., LIU, Y. & XU, J. (1989): Tectonic denudation and the unroofing history of the central Himalayas. *Geol. Soc. Am., Abstr. Programs* **21**(6), A182.

_____ & SILVERBERG, D.S. (1988): Thermal evolution of the greater Himalaya, Garhwal, India. *Tectonics* **7**, 583-600.

_____ & SPEAR, F.S. (1982): Geothermometry, geobarometry, and the Al_2SiO_5 triple point at Mt. Moosilauke, New Hampshire. *Am. Mineral.* **67**, 1118-1134.

HOLDAWAY, M.J. (1971): Stability of andalusite and the aluminum silicate phase diagram. *Am. J. Sci.* **271**, 97-131.

_____ & LEE, S.M. (1977): Fe–Mg cordierite stability in high-grade pelitic rocks based on experimental, theoretical, and natural observations. *Contrib. Mineral. Petrol.* **63**, 175-198.

HOLLISTER, L.S. (1966): Garnet zoning: an interpretation based on the Rayleigh fractionation model. *Science* **154**, 1647-1651.

_____ (1982): Metamorphic evidence for rapid (2 mm/yr) uplift of a portion of the central gneiss complex, Coast Mountains, B. C. *Can. Mineral.* **20**, 319-332.

HONEGGER, K., DIETRICH, V., FRANK, W., GANSSER, A., THÖNI, M. & TROMMSDORFF, V. (1982): Magmatism and metamorphism in the Ladakh Himalayas (the Indus–Tsangpo suture zone). *Earth Planet. Sci. Lett.* **60**, 253-292.

HUBBARD, M.S. (1989): Thermobarometric constraints on the thermal history of the Main Central Thrust Zone and the Tibetan Slab, eastern Nepal Himalaya. *J. Metamorph. Geol.* **7**, 19-30.

_____ & HARRISON, T.M. (1989): $^{40}Ar/^{39}Ar$ age constraints on deformation and metamorphism in the Main Central thrust zone and Tibetan Slab, eastern Nepal Himalaya. *Tectonics* **8**, 865-880.

JAUPART, C. & PROVOST, A. (1985): Heat focussing, granite genesis, and inverted metamorphic gradients in continental collision zones. *Earth Planet. Sci. Lett.* **73**, 385-397.

KENAH, C. & HOLLISTER, L.S. (1983): Anatexis in the Central Gneiss Complex, British Columbia. *In* Migmatites, Melting and Metamorphism (M.P. Atherton & C.D. Gribble, eds.). Shiva Geology Series, Nantwich, U.K. (142-162).

KERRICK, D.M. (1972): Experimental determination of muscovite + quartz stability with $P_{H_2O} < P_{total}$. *Am. J. Sci.* **272**, 946-958.

KOZIOL, A.M. & NEWTON, R.C. (1988): Redetermination of the anorthite breakdown reaction and improvement of the plagioclase – garnet – Al_2SiO_5 – quartz geobarometer. *Am. Mineral.* **73**, 216-223.

KRETZ, R. (1983): Symbols for rock-forming minerals. *Am. Mineral.* **68**, 277-279.

LE FORT, P. (1975): Himalayas: the collided range. Present knowledge of the continental arc. *Am. J. Sci.* **275–A**, 1-44.

_____ (1981): Manaslu leucogranite: a collision signature of the Himalaya. A model for its genesis

and emplacement. *J. Geophys. Res.* **86**, 10545-10568.

_____ (1986): Metamorphism and magmatism during the Himalayan collision. *In* Collision Tectonics (M.P. Coward & A.C. Ries, eds.). *Geol. Soc. London, Spec. Publ.* **19**, 159-172.

MOHAN, A., WINDLEY, B.F. & SEARLE, M.P. (1989): Geothermobarometry and development of inverted metamorphism in the Darjeeling - Sikkim region of the eastern Himalaya. *J. Metamorph. Geol.* **7**, 95-110.

MOLNAR, P. (1984): Structure and tectonics of the Himalaya: constraints and implications of geophysical data. *Ann. Rev. Earth Planet. Sci.* **12**, 489-518.

_____ (1986): The geologic history and structure of the Himalaya. *Am. Scientist* **74**, 143-154.

NEWTON, R.C. & HASELTON, H.T. (1981): Thermodynamics of the garnet - plagioclase - Al_2SiO_5 - quartz geobarometer. *In* Advances in Physical Geochemistry **1** (R.C. Newton, A. Navrotsky & B.J. Wood, eds.). Springer-Verlag, New York (131-147).

PECHER, A. (1989): The metamorphism in the central Himalaya. *J. Metamorph. Geol.* **7**, 31-41.

PERCHUK, L.L. & LAVRENT'EVA, I.V. (1983): Experimental investigation of exchange equilibria in the system cordierite - garnet - biotite. *In* Kinetics and Equilibrium in Mineral Reactions (S.K Saxena, ed.). Springer-Verlag, New York (199-239).

PINET, C. & JAUPART, C. (1987): A thermal model for the distribution in space and time of the Himalayan granites. *Earth Planet. Sci. Lett.* **84**, 87-99.

POGNANTE, U. & LOMBARDO, B. (1989): Metamorphic evolution of the High Himalayan Crystallines in S. E. Zanskar, India. *J. Metamorph. Geol.* **7**, 9-17.

SCHÄRER, U., XU RONG-HUA & ALLÈGRE, C.J. (1984): U-Pb geochronology of Gangdese (Transhimalaya) plutonism in the Lhasa - Xigaze region, Tibet. *Earth Planet. Sci. Lett.* **69**, 311-320.

_____, _____ & _____ (1986): U-(Th)-Pb systematics and ages of Himalayan leucogranites, South Tibet. *Earth Planet. Sci. Lett.* **77**, 35-48.

SEARLE, M.P. & REX, A.J. (1989): Thermal model for the Zanskar Himalaya. *J. Metamorph. Geol.* **7**, 127-134.

SPEAR, F.S. (1991): On the interpretation of peak metamorphic temperatures in light of garnet diffusion during cooling. *J. Metamorph. Geol.* **9**, 379-388.

STÄUBLI, A. (1986): Inverse Metamorphose am Main Central Thrust (NW-Himalaya). *Schweiz. Mineral. Petrogr. Mitt.* **66**, 485-486.

_____ (1989): Polyphase metamorphism and the development of the Main Central Thrust. *J. Metamorph. Geol.* **7**, 73-93.

TRACY, R.J. (1978): High grade metamorphic reactions and partial melting in pelitic schist, west-central Massachusetts. *Am. J. Sci.* **278**, 150-178.

_____ (1982): Compositional zoning and inclusions in metamorphic minerals. *In* Characterization of Metamorphism through Mineral Equilibria (J.M. Ferry, ed.). *Rev. Mineral.* **10**, 355-397.

_____, ROBINSON, P. & THOMPSON, A.B. (1976): Garnet composition and zoning in the determination of temperature and pressure of metamorphism, central Massachusetts. *Am. Mineral.* **61**, 762-775.

TRELOAR, P.J., BROUGHTON, R.D., WILLIAMS, M.P., COWARD, M.P. & WINDLEY, B.F. (1989): Deformation, metamorphism and imbrication of the Indian plate, south of the Main Mantle Thrust, north Pakistan. *J. Metamorph. Geol.* **7**, 111-125.

VIDAL, P., COCHERIE, A. & LE FORT, P. (1982): Geochemical investigations of the Manaslu leucogranite (Himalaya, Nepal). *Geochim. Cosmochim. Acta* **46**, 2279-2292.

WINDLEY, B.F. (1983): Metamorphism and tectonics of the Himalaya. *J. Geol. Soc. London* **140**, 849-865.

WOODSWORTH, G.J. (1977): Homogenization of zoned garnet from pelitic schists. *Can. Mineral.* **15**, 230-242.

YARDLEY, B.W.D. (1977): An empirical study of diffusion in garnet. *Am. Mineral.* **62**, 793-800.

Received January 8, 1991, revised manuscript accepted September 25, 1991.